NASA-CR-172,336

NASA Contractor Report 172336

NASA-CR-172336
19840017633

F-14 MODELING STUDY

W. H. Levison and S. Baron

BOLT BERANEK AND NEWMAN INC.
Cambridge, Massachusetts 02238

Contract NAS1-16738
May 1984

LIBRARY COPY

JUN 26 1984

LANGLEY RESEARCH CENTER
LIBRARY, NASA
HAMPTON, VIRGINIA

National Aeronautics and
Space Administration

Langley Research Center
Hampton, Virginia 23665

TABLE OF CONTENTS

N84-25701#

LIST OF FIGURES

LIST OF TABLES

ABSTRACT

In this report we describe preliminary results in the application of a closed-loop pilot/simulator model to the analysis of some simulator fidelity issues in the context of an air-to-air target tracking task. The closed-loop model is described briefly. Then, problem simplifications that are employed to reduce computational costs are discussed. Finally, model results showing sensitivity of performance to various assumptions concerning the simulator and/or the pilot are presented.

SYMBOLS

$\underline{A}$	transformation matrix
D	distance between target and pursuer
$\underline{I}$	identity matrix
P,p	vehicle roll rate
Q,q	vehicle pitch rate
R,r	vehicle yaw rate
U,u	vehicle velocity along the X body axis
V,v	vehicle velocity along the Y body axis
$\underline{V}$	vector vehicle velocity: [U,V,W]
W,w	vehicle velocity along the Z body axis
X	front-back body axis, positive forward
Y	left-right body axis, positive rightward
Z	vertical body axis, positive downward
δ	control input
θ	Euler pitch angle. Also $\int q$
ϕ	Euler bank angle. Also $\int p$
ψ	Heading angle. Also $\int r$
$\underline{\Omega}$, $\underline{\omega}$	vehicle rotation matrix (defined in text)
μ	line-of-sight angle in elevation
λ	line-of-sight angle in azimuth

subscripts

a	aileron
e	"error" (deviation from trim); Also elevator.

I	refers to inertial coordinate frame
o	steady-state trim condition
p	pilot
P	refers to pursuer body coordinate frame
r	rudder
t	throttle
T	refers to target body

1. INTRODUCTION

Both the military and civilian segments of aviation are placing an increasing reliance on flight simulators for aircraft research and development and for pilot training and proficiency maintenance. This fact, combined with the increasing sophistication and associated costs of available simulation devices, has raised the issues of the numerous trade-offs between simulation fidelity and costs to highly visible levels. In determining the simulation configuration required to meet certain goals, the concerned designer must consider the need for particular cueing devices as well as the requisite level of fidelity. For existing configurations, the simulation user should have some knowledge of the constraints placed upon the man-machine system performance (including performance/workload tradeoffs) by that level of simulation fidelity.

For these reasons, NASA-LaRC has been engaged in a long range, parallel experimental and analytical program to develop data and methodology for evaluation and specification of simulator validity and fidelity. The experimental program has involved in-simulator experiments at the NASA-LaRC facilities to determine the effects on pilot/vehicle performance of digital computation and cueing hardware characteristics [1, 2].

The analytic effort has involved development of a closed-loop model for a real-time digital simulation facility

[3], which incorporates a multi-axis model for the human pilot. This simulation facility model allows simulator design trade-offs to be quantitatively evaluated. The model for the human pilot is a multi-cue version of the optimal control model [4-6] and the simulation facility portion includes the effects of plant discretization, computer iteration rate, interface conversion equipment (A-D and D-A), and hardware system characteristics (e.g. visual delays, force-feel/control loading system, time lags, etc.). This model of a simulation facility, once tuned about the local conditions with data from an in-simulator experiment, can then be used to analyze both hardware and software design increments about these local conditions.

Recent extensions of the model have provided for the dynamics of proprioceptive, kinesthetic, and vestibular cue generation equipment, as well as the informational contributions, ignoring any transformations imposed by the sensory organs involved [6]. However, the motion sensing portion of the model has not been completely tested and in-simulator data has revealed some discrepancies between the data and the pre-experimental predictions of the untuned model [2].

The work described in this report is part of an effort aimed at further development and validation of the analytic model as well as at obtaining a deeper understanding of the effects of simulation inadequacies on human pilots. The effort is both

analytical and empirical with the experimental effort involving both in-simulator experiments with various degrees of cueing (fixed base, platform motion, g-seat) and actual in-flight duplications of the same flight control task. The same pilots are used for simulator and flight experiments. The task involves an F-14 aircraft tracking a target aircraft that is executing a 3g wind-up turn. Once steady state undisturbed tracking has been achieved, the reticle (sight) of the pursuing aircraft is disturbed by a random appearing signal. The simulator experiments duplicate this task under varying cueing conditions (fixed-base, g-seat, helmet loader, platform motion). These experiments provide an opportunity for direct comparison of simulator and flight results and should be an important step in the simulator validation process. The parallel analytic effort should result in an improved, validated closed-loop model and in a greater understanding of how simulator deficiencies affect pilot performance and workload.

Unfortunately, at the time this report was written, the experimental results had not been analyzed. Thus, the report is limited to a discussion of the analytic approach and preliminary model results; it is expected that later reports will present the experimental results and additional model analysis as well.

2. THE CLOSED-LOOP PILOT/SIMULATOR MODEL

The closed-loop pilot simulator model is based on the Optimal Control Model (OCM) for the human operator. The OCM has been documented extensively [4-6] so, here, we will only review it very briefly.

A detailed block diagram of both the system and the OCM pilot model is given in Figure 2.1. Note that the variables in this diagram are generally vectors so that we are modeling a multi-input, multi-output situation. The system portion (outside the dashed box) provides for representations of control stick dynamics, vehicle dynamics, and the dynamics associated with the simulator drive logic (e.g., a motion base washout filter) and its hardware (e.g., the servo drives). As shown, the two inputs to the system are the set of controls generated by the pilot, and the system disturbances which perturb the vehicle states. The set of system outputs is the cue set provided by the simulator to the pilot's various sensory systems. The OCM system modeling approach involves: a) a linearization of the relevant dynamics associated with each of the subsystems; and b), the construction of a state-variable representation of the combined system dynamics.

The state-variable system model includes dynamics associated with all of the subsystems comprising the simulator in addition to those associated with the aircraft itself and its control and

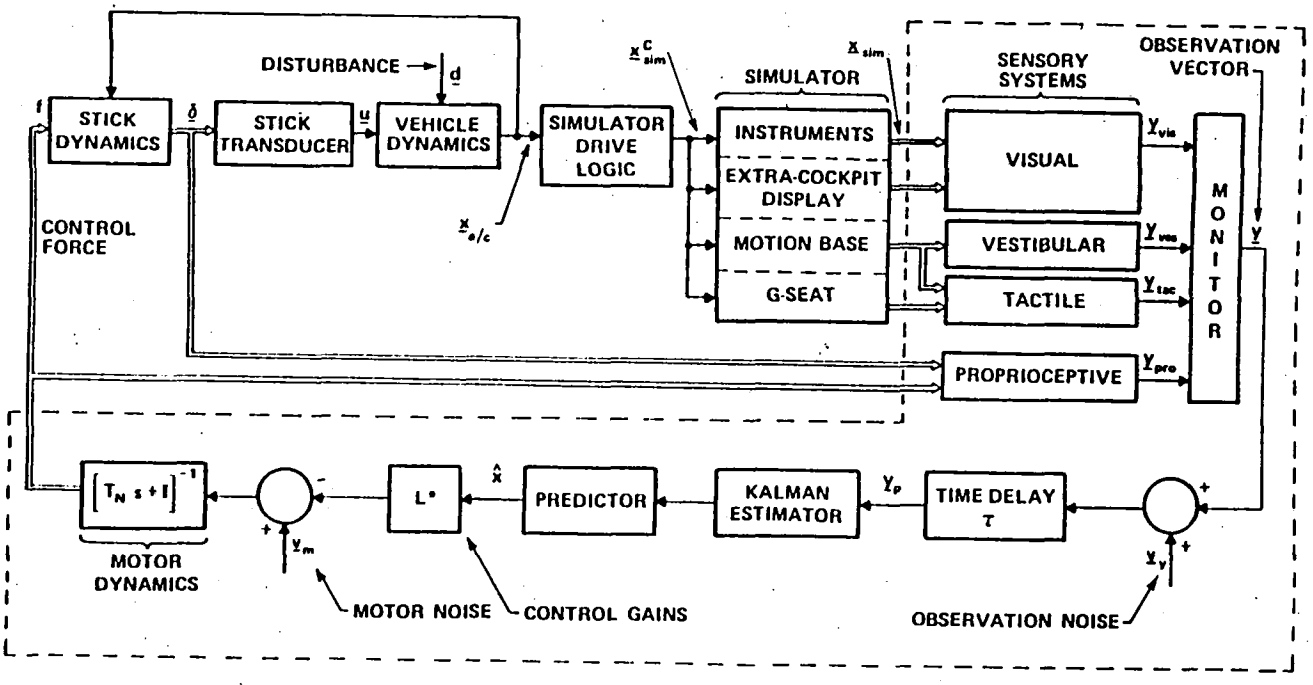

FIG. 2.1 PILOT/SIMULATOR MODEL

display systems. Furthermore, any dynamics (or state variables) needed to model command or disturbance inputs or to account for pilot sensory capabilities (e.g., vestibular dynamics) are included in the formulation as part of this model.* The inclusion of these various elements in the system model is significant because they will then be automatically reflected in the "internal model" of the pilot as represented in the OCM. This is tantamount to assuming that the trained pilot will compensate for predictable correlations in the disturbance inputs and for his own sensory limitations, as well as for the particular (simulator) system being controlled.

It is assumed that the information available to the pilot is that which he obtains via his visual, vestibular, proprioceptive and tactile sensory systems. The individual display vectors associated with a particular modality can include information provided by more than one cueing system which impinge on that same modality. Thus, for example, $\underline{y}_{vis}$ can include both out-the-window (visual) cues and additionally available instrument (visual) cues.

---

* Of course, engineering judgement or more formal analyses will frequently be used to simplify the model significantly. For example, if signal frequency content is well within the bandwidth of a system, the dynamics of that system may be ignored; this is often the case for vestibular dynamics. Such simplifications are very useful in reducing computational costs in applying the OCM and were applied to this problem for the analysis discussed later.

The pilot cannot attend to all sources of information simultaneously and must, therefore, selectively allocate his attention. A model for attention-sharing has been developed and incorporated in the OCM to provide a basis for predicting the effects of attention-sharing on performance [7]. The "monitor" block of Figure 2.1 represents the attention selection portion of the model, i.e., the mechanism for choosing the fraction of attention f_i associated with the ith display variable. (In the steady-state analyses we are conducting, we use the overall or average fractions of attention rather than a moment-to-moment allocation). We assume here that the pilot need not share attention between different sensory modalities; e.g., that processing of, say, motion cues does not interfere with the processing of visual cues. This is a plausible assumption but it has not been validated experimentally; to the extent that the assumption is violated, model results would tend to be somewhat optimistic in predicting the benefits of motion cues. However, attention may have to be shared among the display variables within a particular sensory modality. This is certainly true for the visual modality and could possibly be the case for other modalities. There are two basic approaches to picking the attention levels; either they are computed to optimize performance or, more simply, they are picked by assumption. When the attentions are picked by assumption, it is most frequently assumed that the pilot devotes equal attention to each display;

the attention fraction in that case is the reciprocal of the number of displays.

Additional pilot limitations on the processing of information are accounted for by the time delay and observation noise shown in Figure 2.1. The time delay, τ, is a lumped representation of the various internal delays associated with visual, vestibular, central processing and neuro-motor pathways (typically, 200ms±50ms). Observation noise, $\underline{y}$, is included to account for the pilot's inherent randomness due to random perturbations in human response characteristics and errors in observing displayed variables. A validated model for choosing observation noise covariances exists* [4,7,8].

The optimal estimator, predictor and feedback gain matrix represent the set of "adjustments" or "adaptations" by which the pilot tries to optimize his behavior. The general expressions for these model elements are determined by system dynamics and task objectives according to well-defined mathematical rules (5). The controller is assumed to adopt a response strategy to minimize a cost that is a weighted sum of averaged output and control variances. The most commonly used method for selecting

---

* The model for attention-sharing is used to modify the basic observation noise covariances -- the less attention devoted to a variable, the higher the corresponding observation noise.

reasonable a priori estimates for the cost weightings is to set them equal to the reciprocal of the square root of an "allowable" limit or deviation from nominal in the corresponding system variable; this approach has been described in several recent applications of the OCM (see, for example, [9]. The control-rate related weightings may be chosen in a similar fashion or, as is usually the case, they may be picked to yield a desired values for the neuromotor lag matrix, $\underline{T}_N$ (see Figure 2.1 and below).

Finally, response limitations on the pilot's ability to execute appropriate control actions and to have perfect knowledge of those actions are accounted for in the motor model, which is comprised of the first-order lag matrix $\underline{T}_N$ and a white motor noise source.

3. MODEL FORMULATION OF TASK

As noted earlier, the basic flight task investigated involved an F-14 tracking a target (T-38) aircraft executing a 3g wind-up turn. For this analysis, tracking was to occur at a constant altitude of 10,000 ft. and a constant airspeed of 350 Kts. Steady-state tracking was desired so the chase aircraft was instructed to maintain a constant range (~800'), as well as altitude and airspeed. The pitch, roll and yaw SAS's of the F-14 were operational for the task. The gunsight was displayed on a programmable HUD which was modified to allow the reticle to be driven in elevation by a signal consisting of a sum-of-thirteen sine waves with random initial phasing. The power in the sine waves was chosen so that the discrete spectrum of this signal was an approximation to the continuous spectrum that would obtain from passing white noise through a second order filter (with poles at 0.25 r/s and 0.5 r/s). The pilot "tracked" by keeping the reticle on the target.

The analytic description of this task involves a very high order state-variable formulation; without any approximations, the implementation of the augmented (i.e., including SAS) F-14 vehicle dynamics requires 24 state variables, and eight additional state variables are needed for the display of target

position.* There are four possible pilot control inputs (including the throttle for speed control). A problem of this magnitude represents a significant computational burden in the OCM context that will assume even greater import when model results are to be matched or tuned with data, as will be required later.

In order to minimize the potential computational costs and problems, efforts were made to reduce the size of the system model without compromising the fidelity of the model response. The specific simplifications made, and their justification, are discussed in some detail below. Briefly, system model simplification proceeded in the following stages. First, the LOS equations given in Appendix A were simplified. Then, the control/stability augmentation system was greatly reduced. Finally, additional simplifications were made for obtaining closed-loop predictions with the OCM. This led to a 16-state, two-control model ultimately being used for predicting pilot/vehicle performance. This reduction in system complexity leads to very substantial computational savings. The reduced order equations are given in Appendix C.

---

* The display or line-of-sight (LOS) equations are given in Appendix A, target kinematics are derived in Appendix B, and system state equations are given in Appendix C.

Simplification of LOS Equations

Initial exploration with the BBN model response indicated that the LOS equations (see Appendix A) could be simplified without materially affecting model response. For the model tests described here, and for all subsequent model applications, the target u-state, and the LOS-related θ- and ϕ-states were eliminated from the state-variable representation. Furthermore, the Euler θ-state was used in computing LOS error, rather than the "local" θ-state as defined in the Appendix.

This (partially) reduced-order model was verified through a comparison of the open-loop transient resonses of the analytic and simulation models. In order to provide a transient response that would exhibit some of the variational behavior typical of closed-loop tracking and that would avoid the build-up of very large "errors", pitch and roll triplets were used as inputs. The δ_{e_p} and δ_{a_p} trajectories used in this verification are shown in Table 3.1. (Variables of the form δ_{ep} represent "pilot" inputs to the augmented vehicle -- not control surface deflections.)

Near-perfect matches to responses of the vehicle states were achieved by the BBN computer model. Sample tracings of model (smooth curve) and simulator (discrete points) responses are given in Figure 3.1 for pitch rate and in Figure 3.2 for yaw rate. Responses to other state variables were matched equally

TABLE 3.1 TRIPLET INPUTS USED IN COMPUTER MODEL VERIFICATION

Time (sec)	δ_e (in)	δ_a (in)
1.Ø	Ø.4	Ø.25
2.Ø	-1.2	Ø.75
3.Ø	1.2	-Ø.75
4.Ø	-Ø.4	Ø.25

well. In these and ensuing figures, "simulator" refers to the LaRC nonlinear simulation model, and "model" refers to the BBN linear analytic model.

Figures 3.3 and 3.4 show good correspondence between model and simulator LOS errors, for the first 5 seconds following input initiation, for the "on-axis" errors (i.e., response of elevation error to δ_e, and response of azimuth error to δ_a). The responses of azimuth error to δ_e correspond over a smaller range -- about 2 to 3 seconds following onset of the input. Least well matched is the response of the elevation error to the δ_a input. The off-axis responses are relatively small compared to the on-axis responses, however. Overall, the transient response of the BBN model is sufficiently close to that of the LaRC simulation to warrant its use in prediction of closed-loop performance trends.

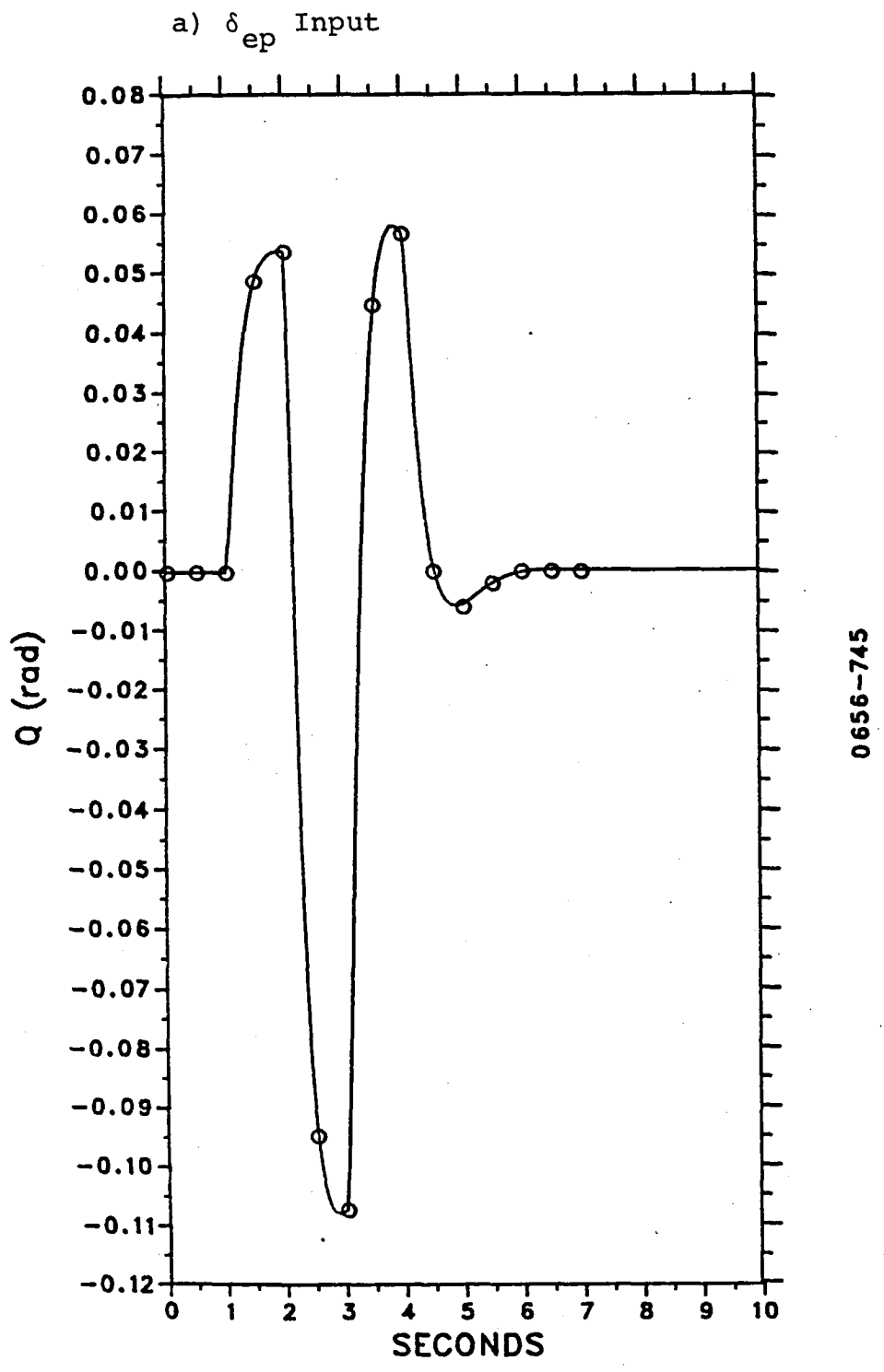

Figure 3.1. Comparison of Model Pitch-Rate Response to Simulator Response

b) δ_{ap} Input

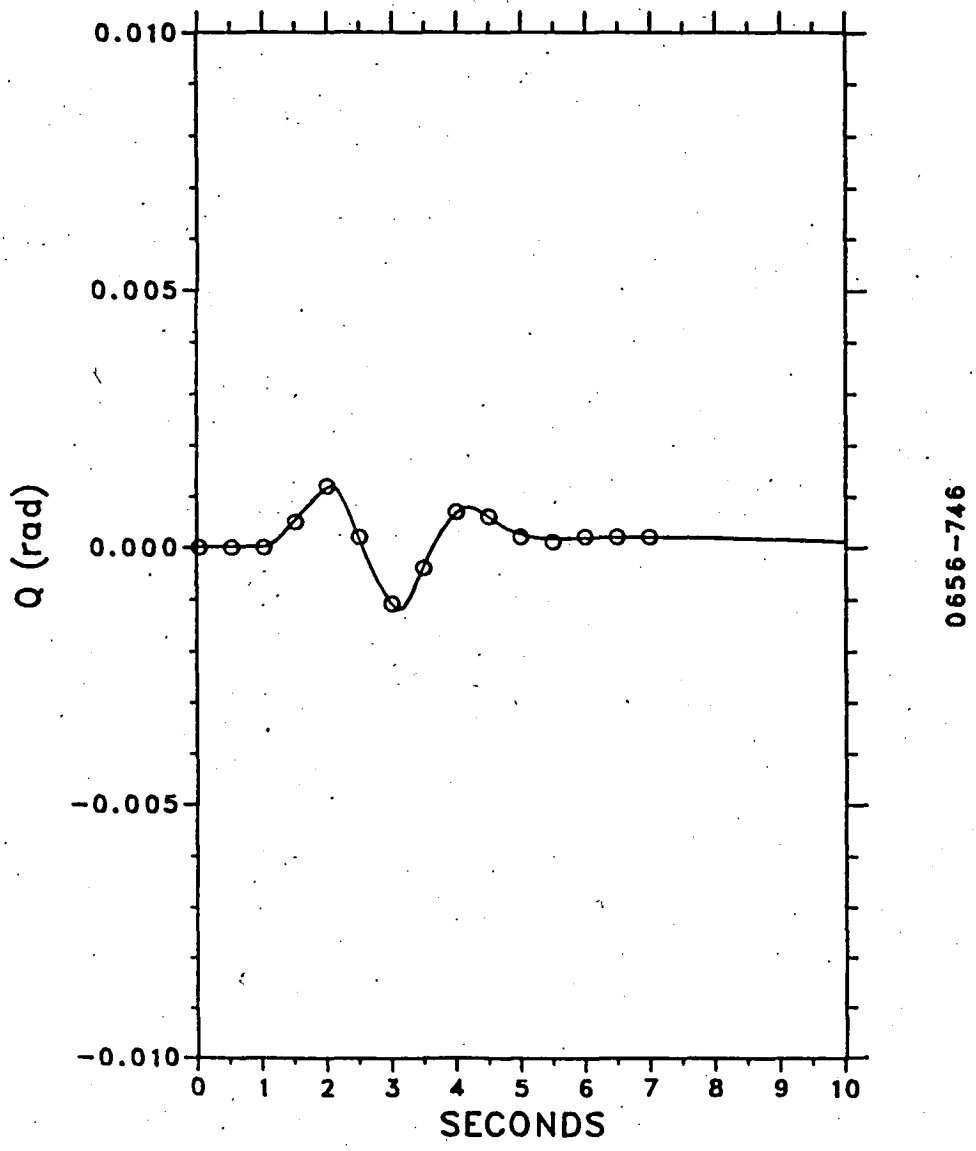

Figure 3.1. (Concluded).

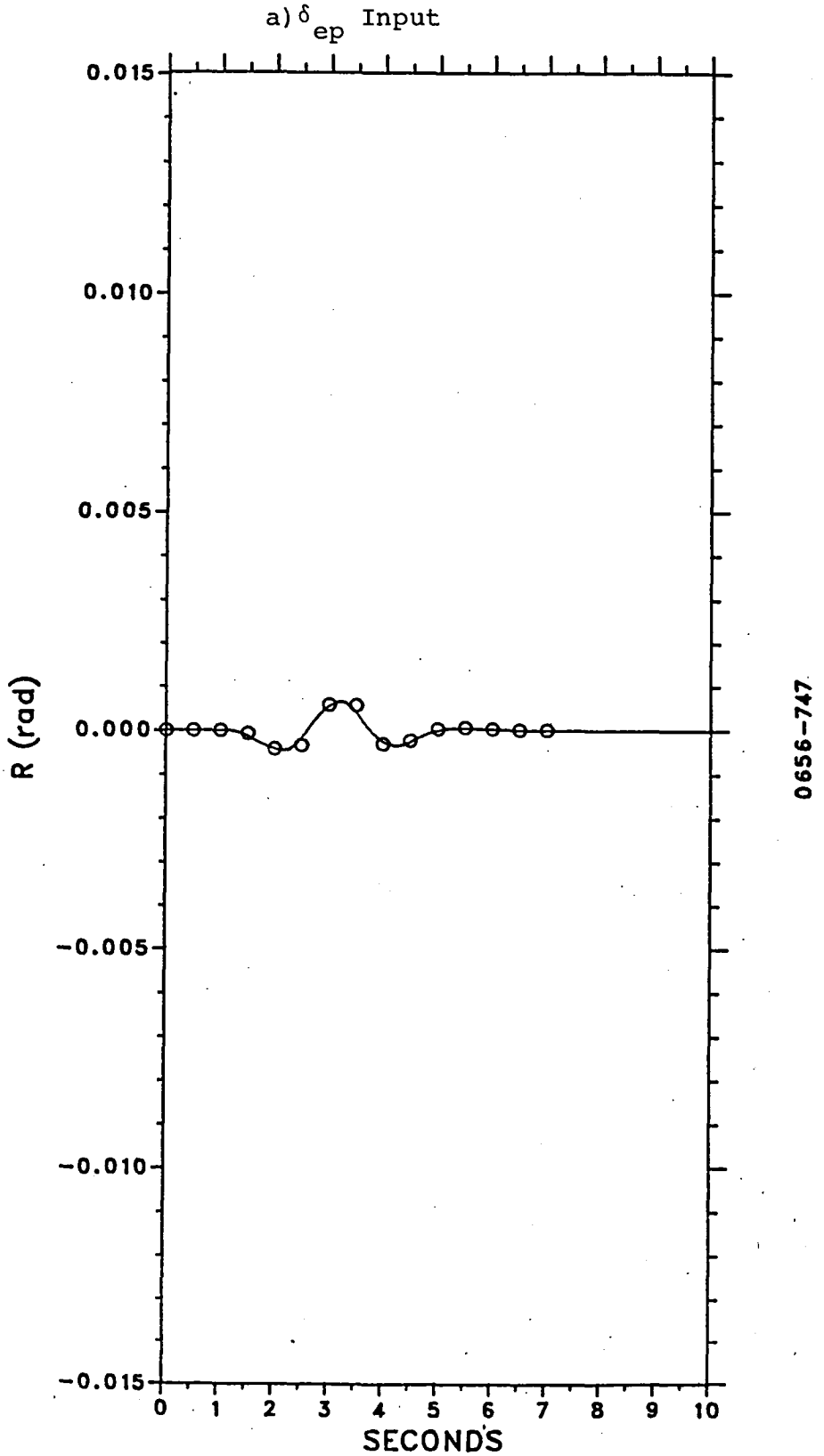

Figure 3.2. Comparison of Model Yaw-Rate Response to Simulator Response

b) δ_{ap} Input

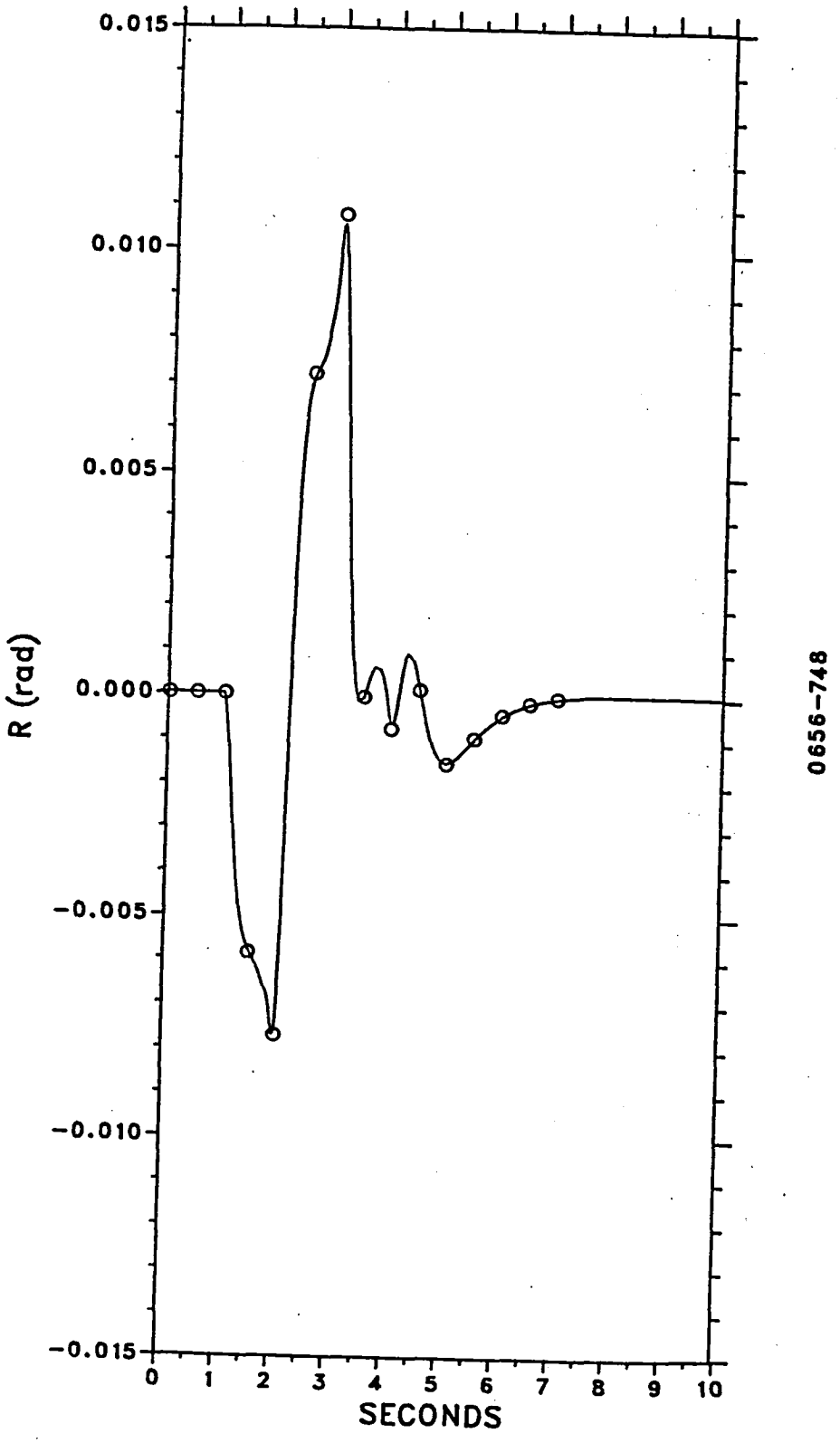

Figure 3.2. (Concluded)

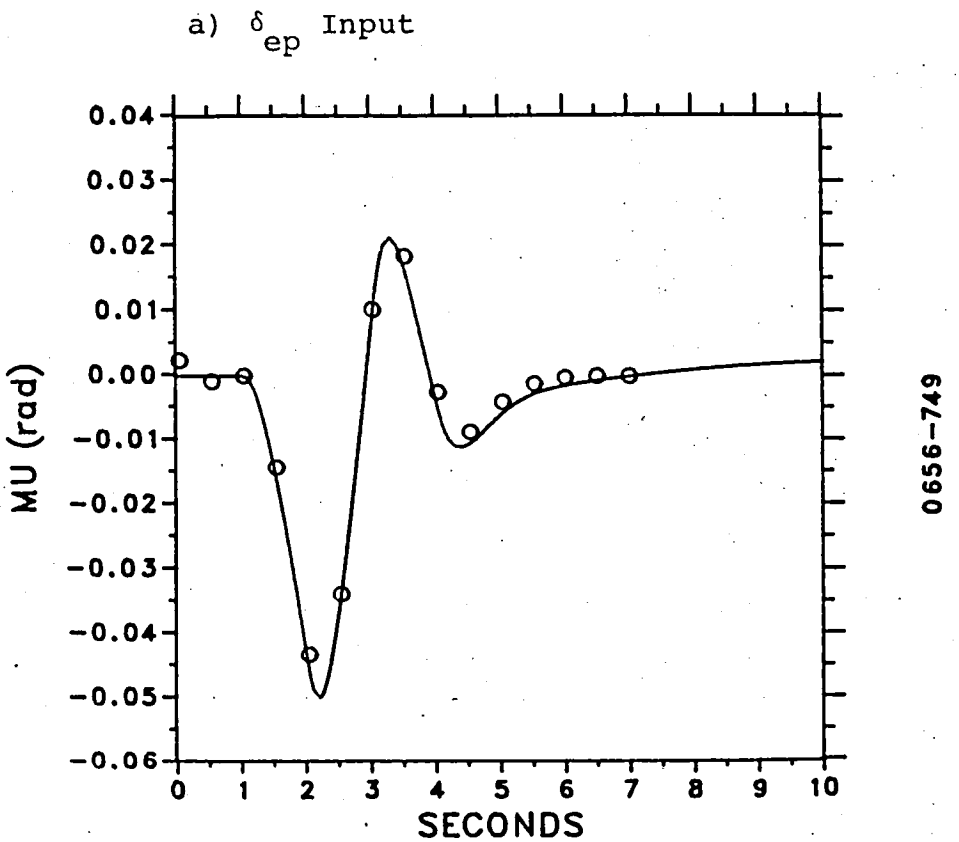

Figure 3.3. Comparison of Model LOS Response in Elevation to Simulator Response

b) δ_{ap} Input

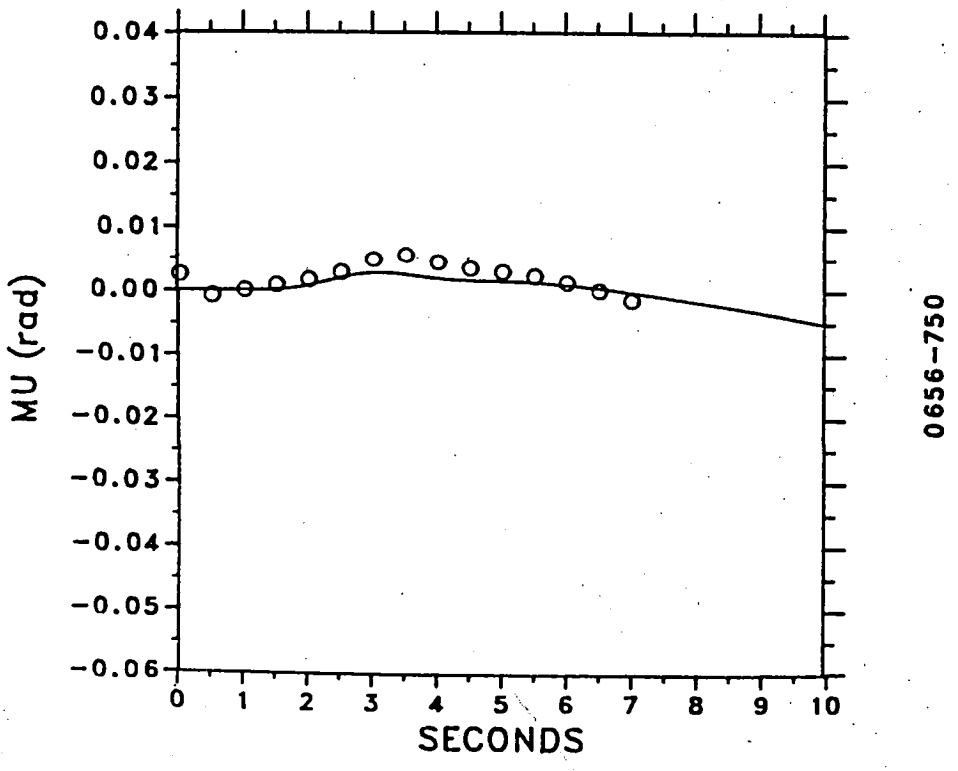

Figure 3.3. (Concluded)

a) δ_{ep} Input

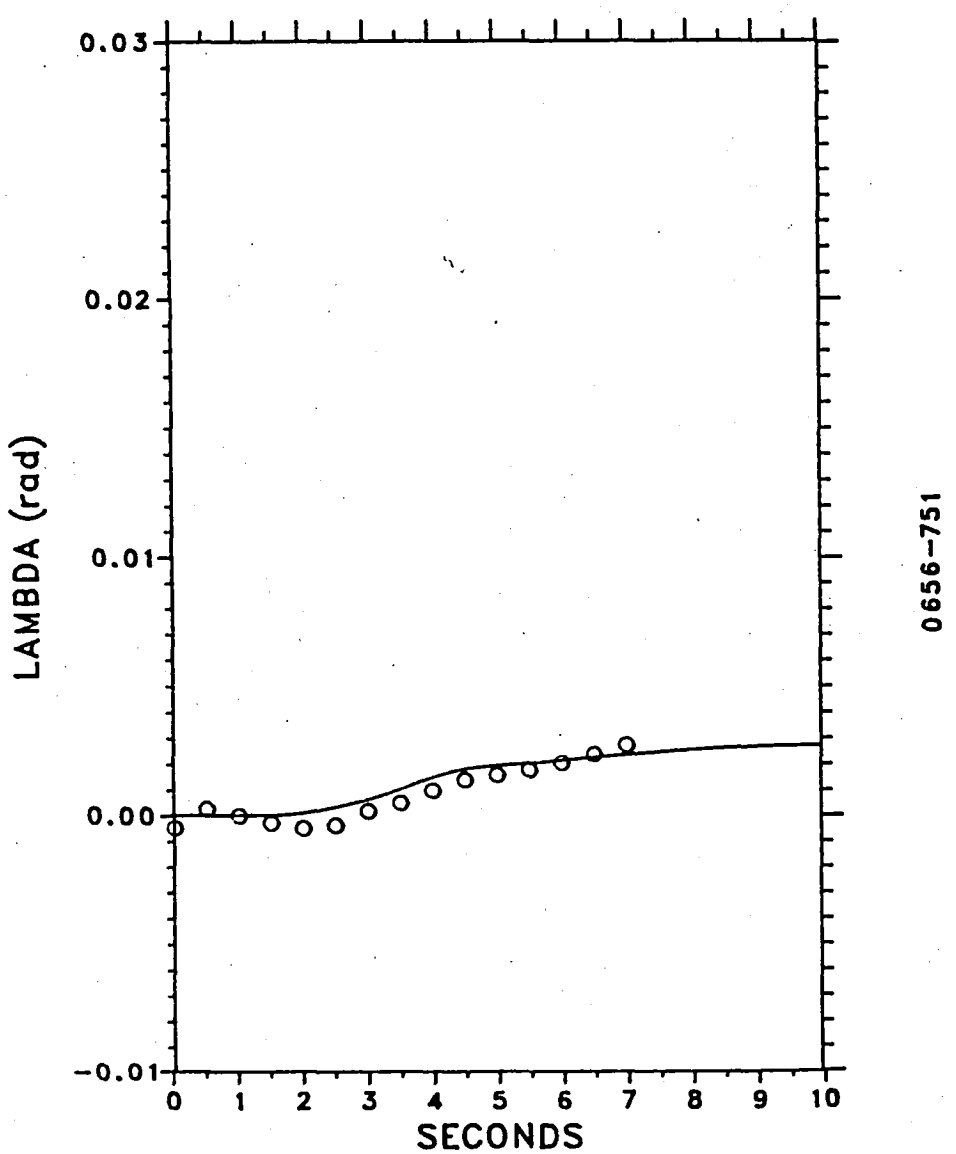

Figure 3.4. Comparison of Model LOS Response in Azimuth to Simulator Response

b) δ_{ep} Input

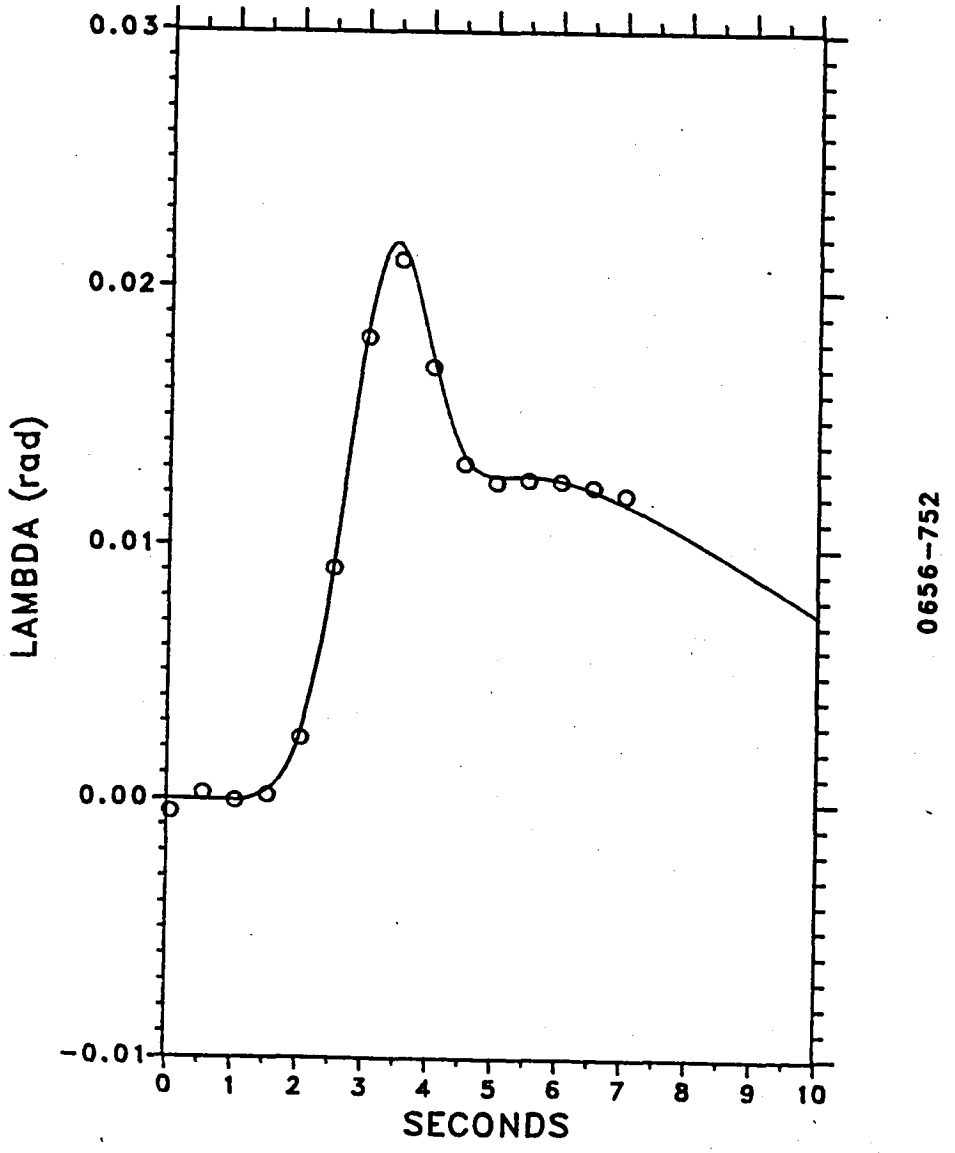

Figure 3.4. (Concluded)

Order Reduction of the Control System

Various factors facilitated order-reduction of the F-14 control/stability augmentation system for purposes of pilot-vehicle performance analysis. First, a number of system elements were simple lags with relatively short time constants (and therefore little effect on vehicle response over the region of man/machine response bandwidth). Second, some redundancies existed in the original definition of control system state variables. Third, other state variables were not excited by the inputs expected in the particular problem under study. Finally, the control system structure was decoupled along the various control axes; this factor allowed us to explore the input/output behavior of the control system individually in each control axis.

Bode plots were computed relating each control-system output to each control-system input, and low-order matches to these bode plots were obtained by gradient search procedures. The reduced-order system eventually adopted contained three state variables (instead of sixteen) to represent a washout in the pitch-rate control loop, a lag-lead network in the roll-rate control loop, and a washout in the yaw-rate control loop. Engine dynamics and control were represented by a pure-gain feedback/feedforward network.

Figures 3.5 and 3.6 compare the elevation and azimuth LOS error transient responses of the augmented vehicle using the

full-state and 3-state augmentation systems. The input trajectories defined in Table 3.1 were used for this comparison. This analysis was performed with the BBN analytic model, with the LOS equations simplified as described above. The transient responses of the two model formulations were in very good agreement.

Whereas these transient responses allow the reader to compare relatively long-term response behaviors, a comparison of short-term response characteristics of the two model formulations can be inferred from the high-frequency portions of the Bode plots shown in Figures 3.7 and 3.8. Four Bode plots are shown, relating azimuth and elevation LOS errors to δ_e and δ_a inputs.

The two model formulations yielded Bode plots that were nearly identical except for high-frequency phase differences found in three of the transfers. In all three cases, the reduced-order system showed less high-frequency phase lag than the full-order system. To compensate for this in computing closed-loop performance, a pure time delay was included in the system description to provide additional high frequency phase lag.

Other Simplifications of System Model

The problem formulation was further simplified by assuming that the pilot could maintain constant range and that variations

a) δ_{ep} Input

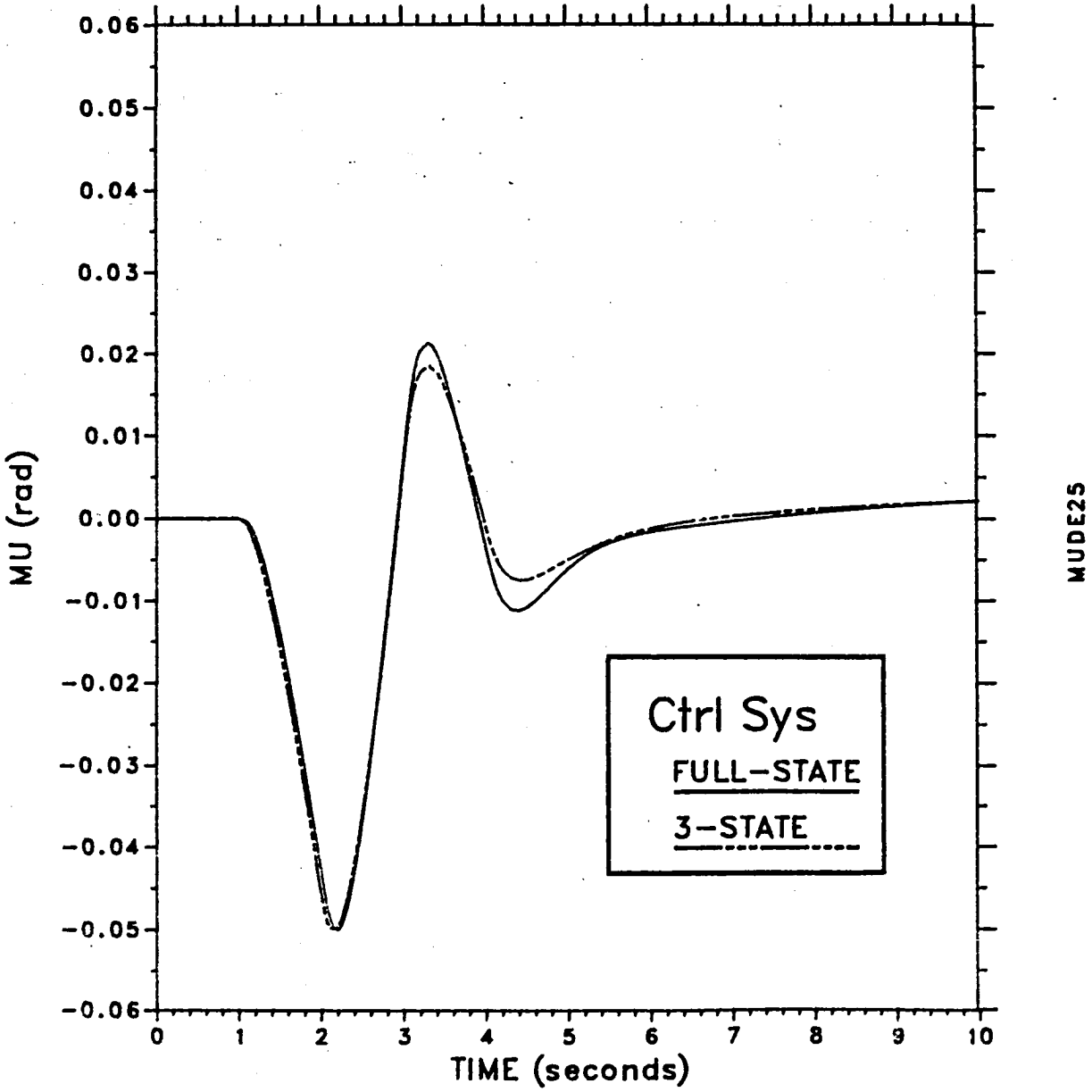

Figure 3.5. Comparison of the Elevation LOS Error Transient Responses of the Full-State and 3-State Augmentation Systems

b) δ_{ap} Input

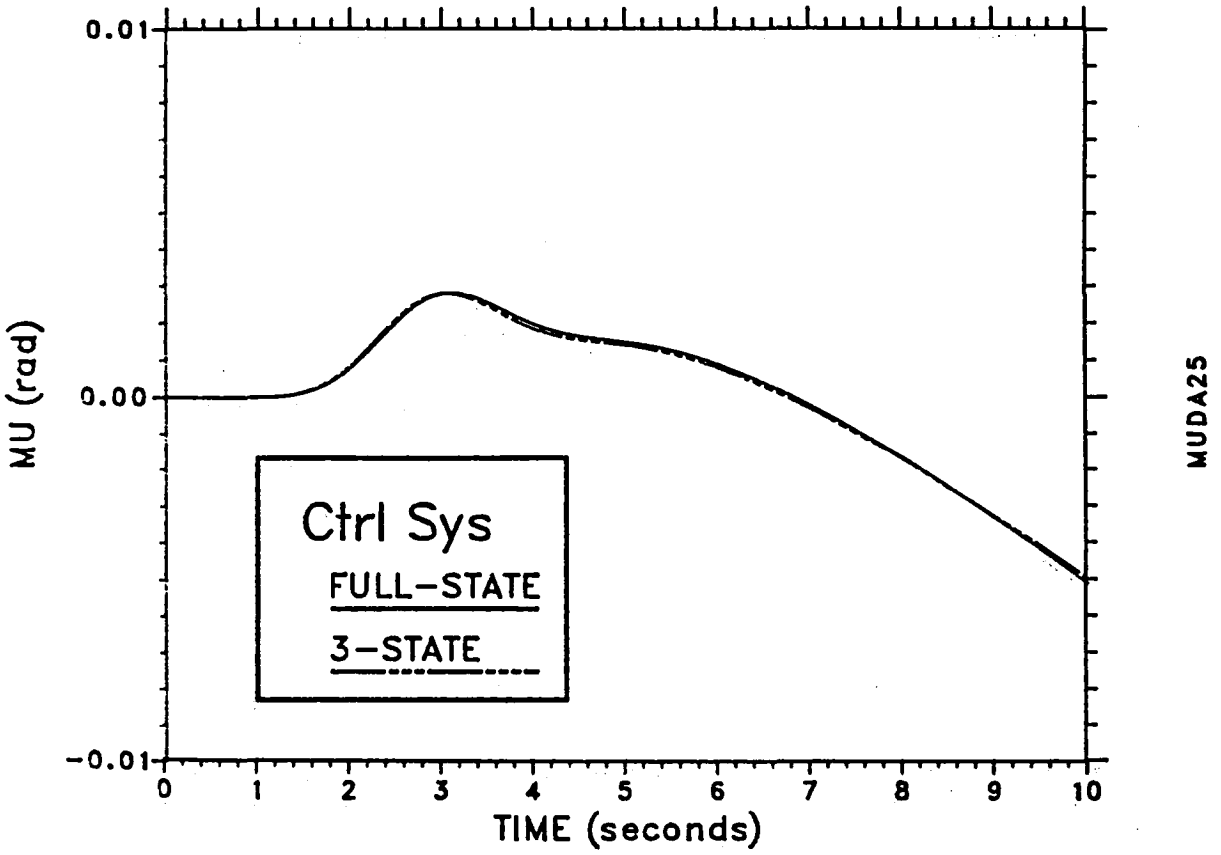

Figure 3.5. (Concluded)

a) δ_{ep} Input

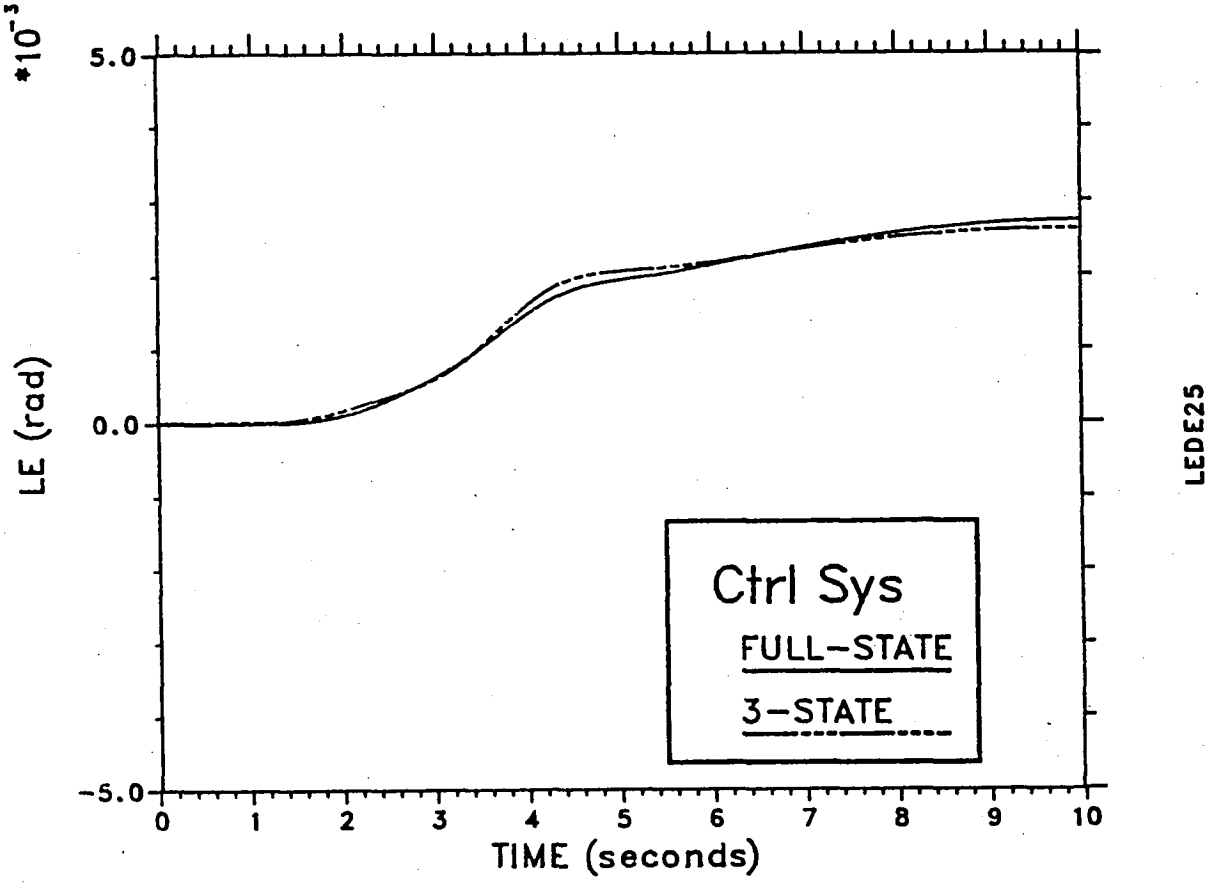

Figure 3.6. Comparison of the Azimuth LOS Error Transient Responses of the Full-State and 3-State Augmentation Systems

b) δ_{ap} Input

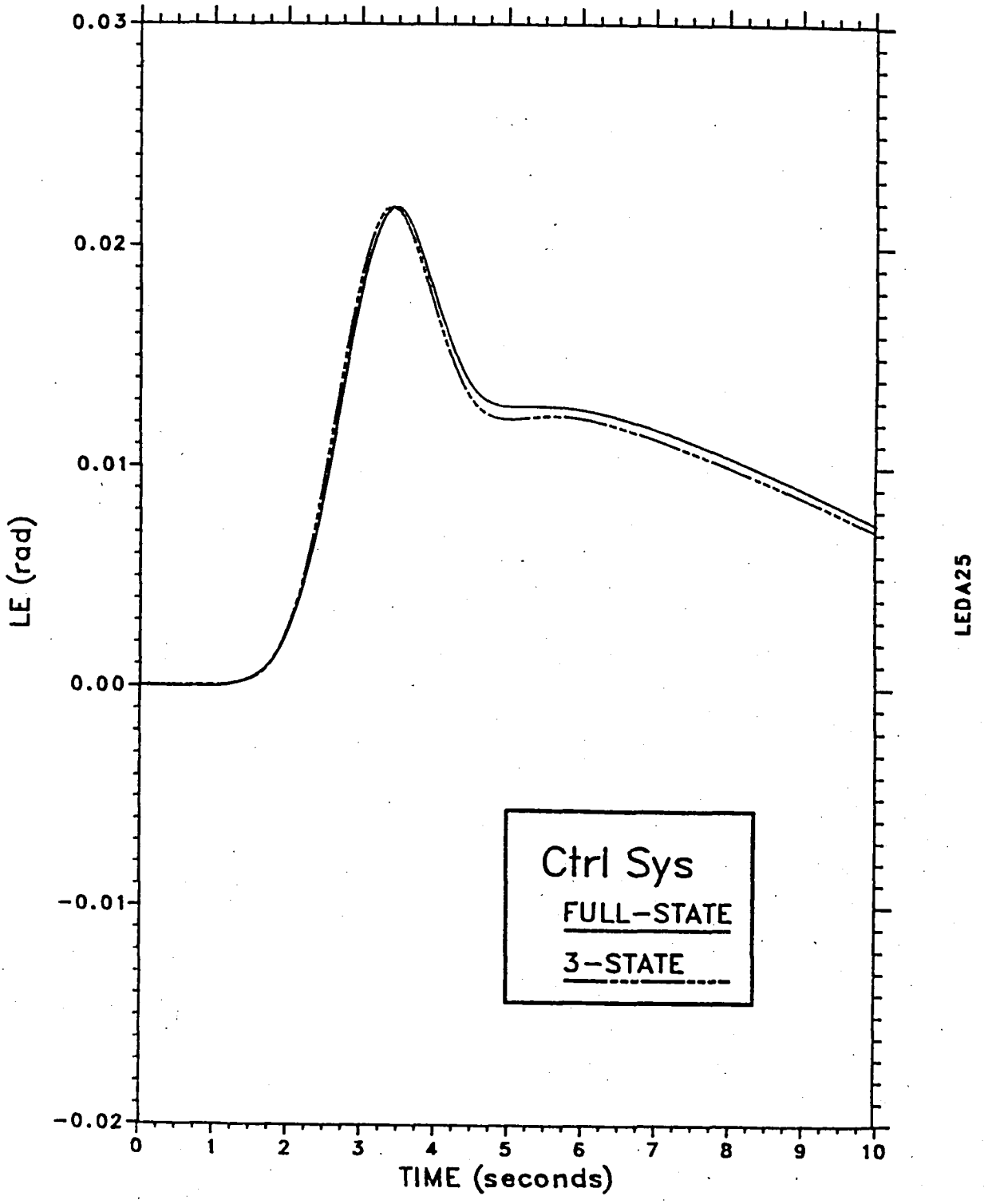

Figure 3.6. (Concluded)

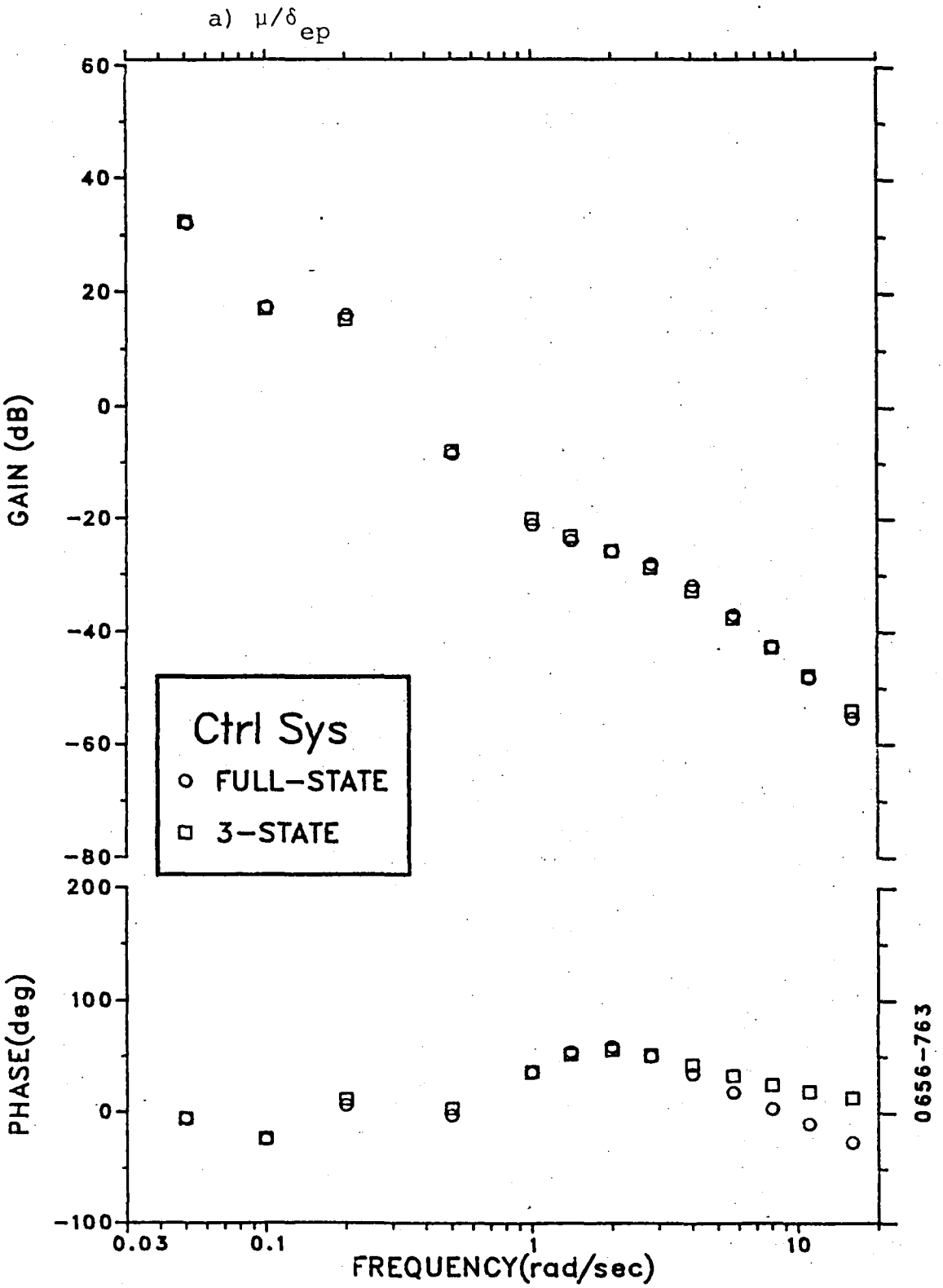

Figure 3.7. Bode Plots Relating Elevation LOS Error to Pilot Control Input

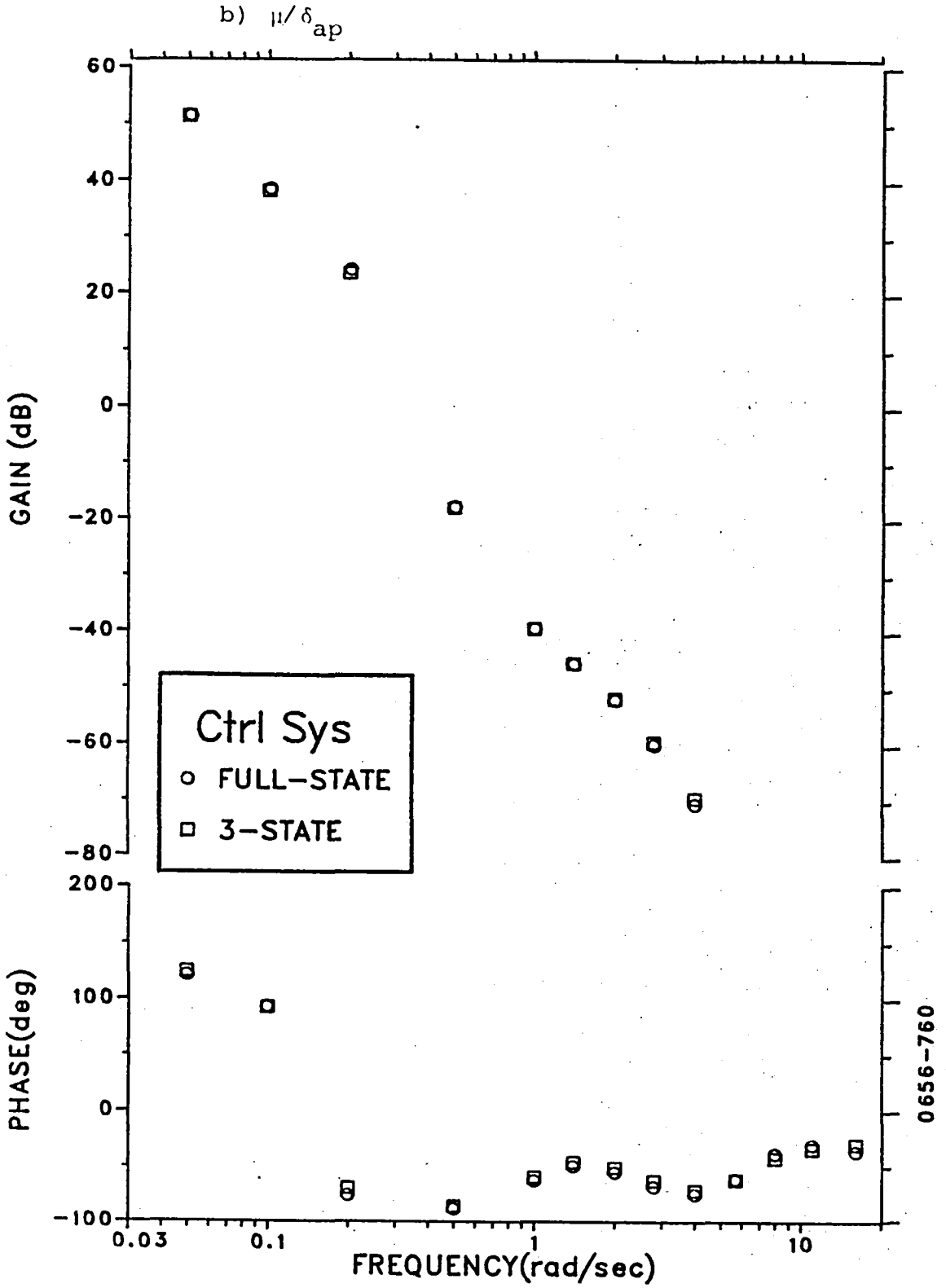

Figure 3.7. (Concluded)

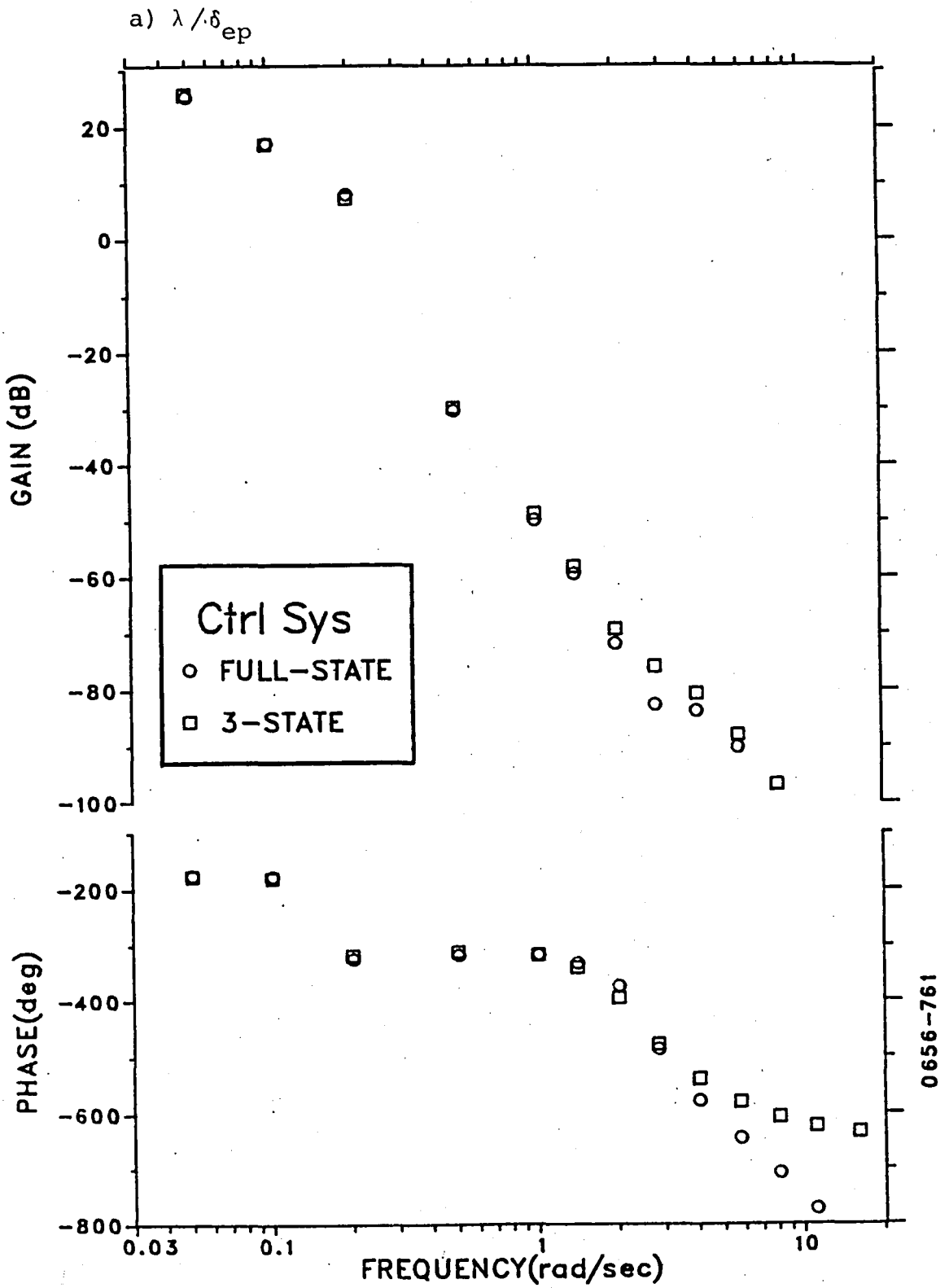

Figure 3.8. Bode Plots Relating Azimuth LOS Error to Pilot Control Input

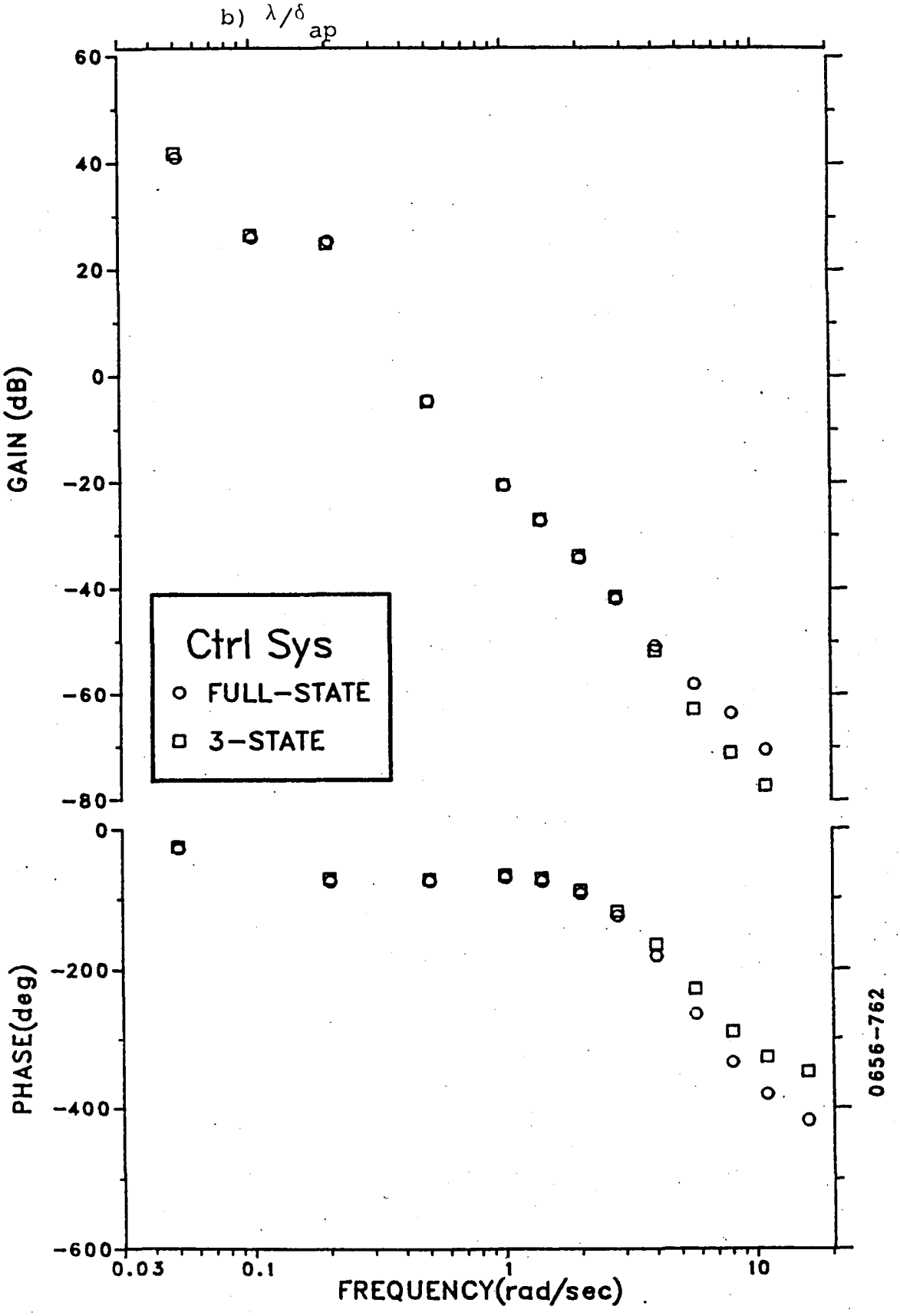

Figure 3.8. (Concluded)

from nominal airspeed could be neglected. It was also found that the number of controls could be reduced to two by assuming constant (equilibrium) thrust and rudder deflection. The effects of these simplifications on predictions of closed-loop performance are discussed in Chapter 4. Finally, for purposes of this preliminary model analysis, human vestibular dynamics were ignored and simulator dynamics were approximated by pure delays.

4. RESULTS AND DISCUSSION

The Optimal Control Model (OCM) was employed prior to the simulation experiments to generate predictions of closed-loop system performance and pilot response behavior. Of particular interest for this analysis were predictions of performance trends concerning the effects (or lack thereof) of the motion- and visual-cueing devices to be explored in the simulation study.

In order to obtain model predictions it was necessary to specify four categories of independent ("pilot-related") model parameters: (a) "cost" coefficients, representing the pilot's perception of control-task requirements; (b) observation noise variables, reflecting attentional and perceptual limitations, as well as limits on the pilot's ability to generate noise-free responses; (c) a time delay reflecting various sources of perceptual, central processing, and execution delays; and (d) a motor noise/signal ratio to account for limits on the pilot's knowledge of vehicle response behavior.

Cost coefficients were determined by first specifying desired "limits" (maximum allowable errors) on important control and response variables, and then setting each quadratic cost coefficient equal to the square of the reciprocal of its corresponding limit. Limits (and therefore "costs") were associated with LOS and airspeed errors, control deviations from trim, and rate-of-change of control (the latter required by the

particular mathematical formulation of the OCM). By assigning zero costs to deviations in other variables, such as attitude changes, the flight task was modeled as a two-variable tracking task.

The pilot was assumed to adopt the radius of the reticle (50 mils, or 2.87°) as the maximum allowable LOS error. Other limits, and associated cost coefficients, are shown in Table 4.1. Cost coefficients for control-rate variables were not set on the basis of assumed limits, but rather on the basis of pilot bandwidth considerations. These coefficients were selected in an iterative fashion to yield "motor time constants" of 0.1 seconds for longitudinal and lateral stick inputs, and 0.2 seconds for rudder and throttle inputs.

Three types of observation noise variables were selected. First, an overall noise/signal ratio was selected as a "free" parameter of the analysis to reflect overall attention to the flight task [6,7]. Second, noise parameters reflecting a statistical treatment of perceptual "threshold" effects were associated with each display variable used by the pilot. Finally, a specific allocation of attention among these display variables was assumed.

The pilot was assumed to use LOS error information (both displacement and rate), as well as airspeed information. "Indifference thresholds" of 1 tick mark (10 mils or 0.57°) were

TABLE 4.1 INITIAL SELECTION OF PILOT MODEL PARAMETERS

Variables	Limit	Cost Coefficient	Threshold	Attention
Display Variables				
μ_e (deg)	2.87	0.12	0.57	0.45
$\dot{\mu}_e$ (deg/sec)	--	0	0.2	0.45
λ_e (deg)	2.87	0.12	0.57	0.45
$\dot{\lambda}_e$ (deg/sec)	--	0	0.2	0.45
$\mu_{\dot{e}}$ (ft/sec)	10	0.01	3.4	0.10
Control Variables				
δ_{ep} (in)		4	0.63	
$\dot{\delta}_{ep}$ (in/sec)		*	*	
δ_{ap} (in)		3.5	.082	
$\dot{\delta}_{ap}$ (in/sec)		*	*	
δ_{rp} (in)		3.0	0.11	
$\dot{\delta}_{rp}$ (in/sec)		*	*	
δ_T (%)		0.5	4.0	
$\dot{\delta}_T$ (%/sec)		*	*	

*Control-rate cost coefficients chosen to yield motor time constants of 0.1 for δ_{ep} and δ_{ap}, and 0.2 for δ_{rp} and δ_t.

associated with the use of LOS error information, and visual thresholds of Ø.2 deg/sec were assumed for LOS error rates. An indifference threshold of 2kt = 3.4 ft/sec was assumed for airspeed regulation. The pilot was assumed to allocate 45% of his available attention to elevation LOS error and error-rate, collectively; another 45% to azimuth LOS error and error rate; and the remaining 1Ø% to airspeed, primarily for cross-checking purposes.

Cost coefficients and perceptual parameters are shown in Table 4.1. In addition, a baseline observation noise/signal ratio of -2ØdB was selected to reflect a situation of moderate-to-high attentional workload; the time delay was set to Ø.32 to reflect the combined effects of inherent operator delay (Ø.2 sec), sample-and-hold operations in generating the visual display (.Ø5 sec), and corrections to the reduced-order augmented vehicle model (.Ø7 sec); and the motor noise/signal ratio was set to -6Ø dB.

Preliminary model analysis was performed to determine the extent to which the problem formulation could be further simplified by reducing the number of active controls, and by eliminating the airspeed state, without compromising the reliability of the model predictions. Three sets of model results were obtained using the relevant parameter settings of Table 4.1: (1) δ_{ep}, δ_{ap}, and δ_{t} active, with airspeed included;

(2) δ_{ep} and δ_{ap} active, with airspeed omitted; and (3) δ_{ep} and δ_{rp} active with airspeed omitted. (Numerical difficulties prevented a model solution with all four controls active.)

These model variations resulted in a spread of less than 10% in each of the predicted LOS error and error-rate variables and in the δ_{ep} control variable. We therefore felt that predictions of performance trends would not be compromised by the selection of one of the simpler model formulations. The configuration with the δ_{ep} and δ_{ap} controls, and without the airspeed state, was used for the remaining pre-experiment model analysis.

The effects of model parameter manipulations on standard deviation (SD) scores* were then predicted. For economy of notation, we define the terms "elevation error" to mean the elevation component of the line-of-sight error, "azimuth error" to mean the azimuth component of the line-of-sight error, and "LOS error" as the vector line-of-sight error. Thus,

$$\sigma_{LOS} = (\sigma_{\mu}^2 + \sigma_{\lambda}^2)^{1/2} .$$

The baseline model configuration was defined using the parameters shown in Table 4.1 with the following exceptions: (1) no rudder and throttle controls, (2) no speed state, and (3)

---

*The steady-state implementation of the OCM used in this study considers all variables as zero-mean processes. Thus, only the variational (SD) statistics of the time histories are predicted.

relative attentions of Ø.5 each to azimuth and elevation LOS error. Predicted standard deviation (SD) scores for this configuration are shown in Table 4.2. Note that the azimuth error is the same order of magnitude as the elevation error, even though the external forcing function (pipper disturbance) is applied only to the elevation component. This result reflects two factors: (1) the coupling between elevation and azimuth in the system equations of motion for the high-bank attitude, and (2) the indifference threshold assigned to azimuth and elevation errors, which turned out to be about the same as the predicted elevation SD score). (Because threshold effects are represented stochastically by observation noise components, rather than deterministically by nonlinear response elements, the predicted SD score can be less than the assumed threshold, as was the case for the predicted azimuth score).

TABLE 4.2 PREDICTED SD SCORES FOR BASELINE CONFIGURATION

Variable	Predicted Score
σ_{LOS}	Ø.69
σ_{μ_e}	Ø.58
σ_{λ}	Ø.38
$\sigma_{\delta ep}$	Ø.21
$\sigma_{\delta ap}$	Ø.13

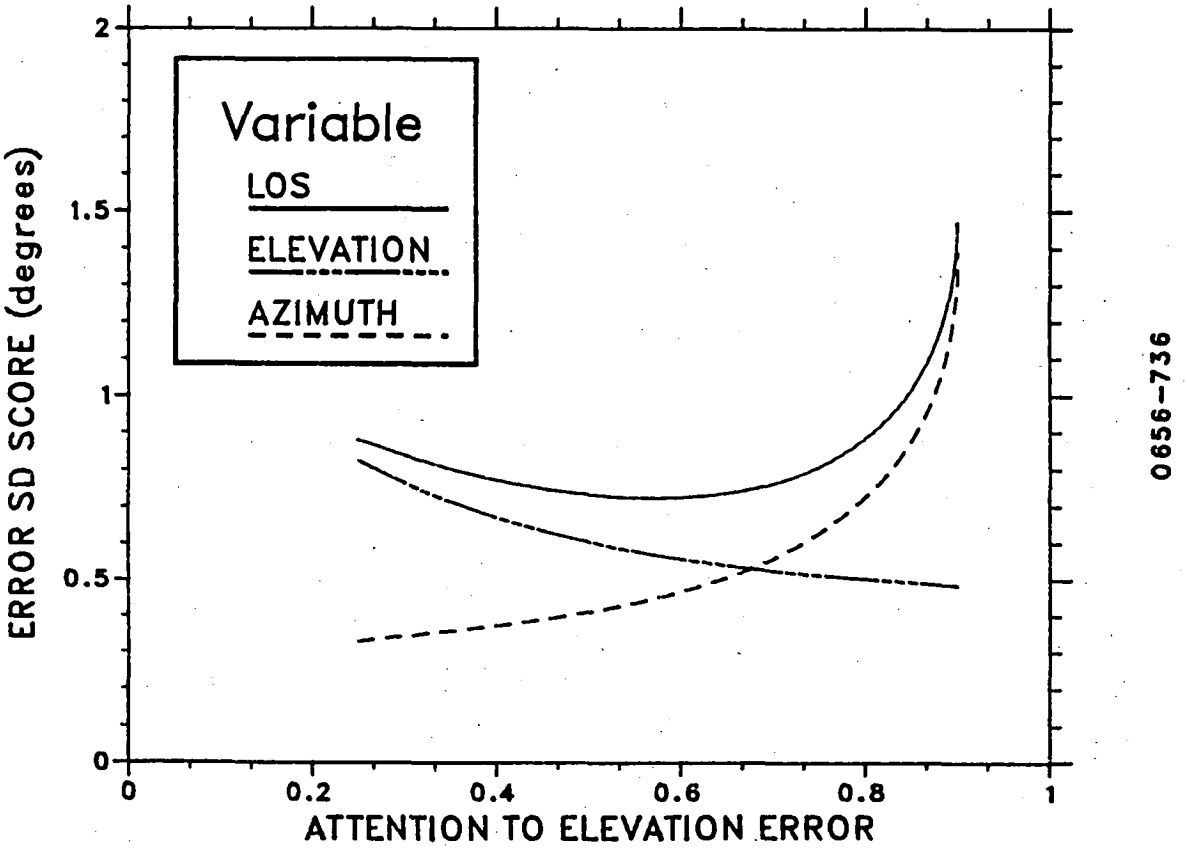

Figure 4.1. Effect of Attention on Predicted Error Scores

The assumed split of attention between elevation and azimuth error components was varied in order to determine the sensitivity of the predicted (vector) LOS error to attentional allocation. Figure 4.1 shows that, while the individual error components were sensitive to attention, they tended to vary in a compensating manner, with the result that the total (vector) LOS error was relatively insensitive to attention in the region of optimal attention-sharing. In particular, the baseline assumption of equal attention to azimuth and elevation errors yielded a LOS error score within 5% of the score obtained with optimal allocation. Since we had no basis for predicting how elevation and azimuth errors would be traded off within the band of insensitivity, the assumption of equal attention-sharing was retained for subsequent model analysis.

Sensitivity analysis was performed with respect to each of the following independent model parameters: (1) observation noise/signal ratio, (2) motor noise/signal ratio, and (3) time delay. This analysis was performed primarily to determine how critically the model predictions depend on the particular selection of parameter values. Because observation noise/signal ratio has been identified with attention [7], the relation between performance and this parameter has the additional interpretation of a performance/workload tradeoff.

Figure 2.2 shows that a 6dB increase in observation noise

(which we interpret as a 75% reduction in attention) caused the predicted LOS error score to approximately double. This sensitivity is greater than that typically predicted for either laboratory tracking or simulated flight tasks [9-11]. If, as suggested by Wewerinke [9], we consider workload to be related to the sensitivity of performance to observation noise, as well as to the average noise level at which the pilot operates, the curves of Figure 4.2 suggest that we are dealing with a relatively high-workload task.

By way of contrast, Figure 4.3 shows that predicted LOS error score is relatively insensitive to motor noise/signal ratio over the range explored. Thus, selection of this parameter is not critical, provided we stay in the range typical of previous studies (between -50 and -60dB).

Sensitivity of performance with respect to time delay was explored, in part, to determine the potential effects of simulator delays. The time delay parameter was varied over a range of 270 to 370 milliseconds, where 270 msec represents a basic operator delay of 200 msec plus 70 msec to account for model simplifications, but no simulator delays. Figure 4.4 shows that predicted LOS error was relatively insensitive to time delay, varying by less than 15% over the range explored. These model results suggest that delays associated with generating visual and motion cues (provided they are less than 100 msec)

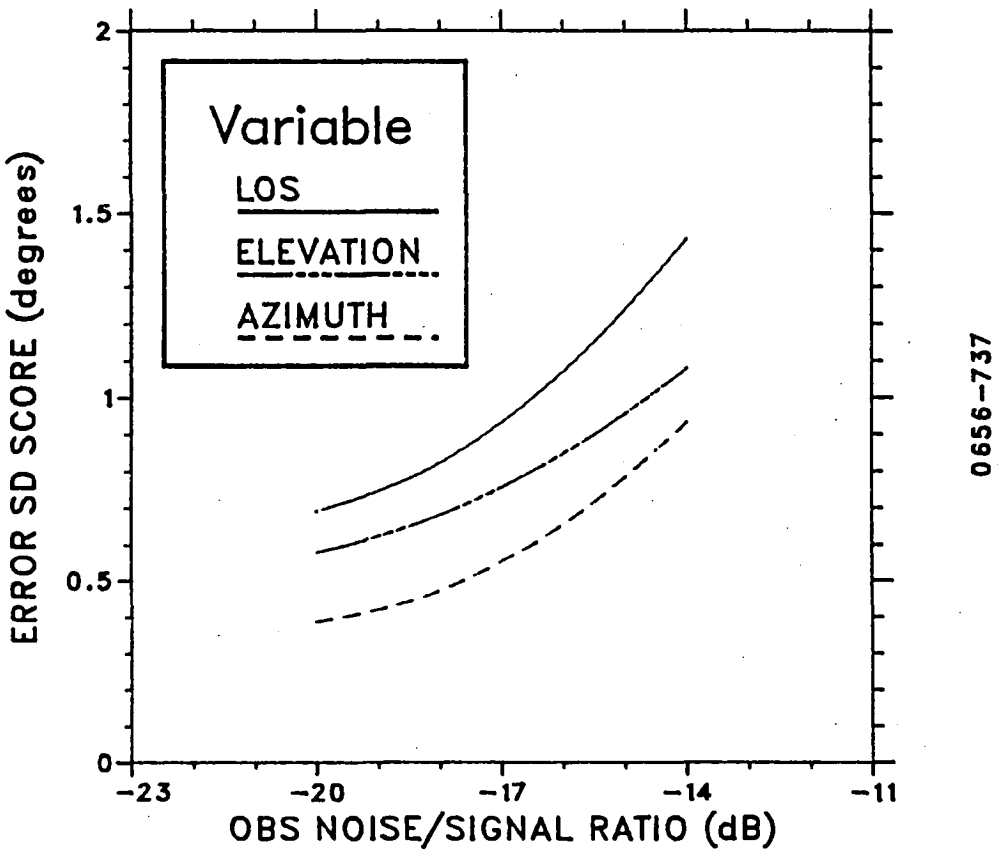

Figure 4.2. Effect of Observation Noise/Signal Ratio on Predicted Error Scores

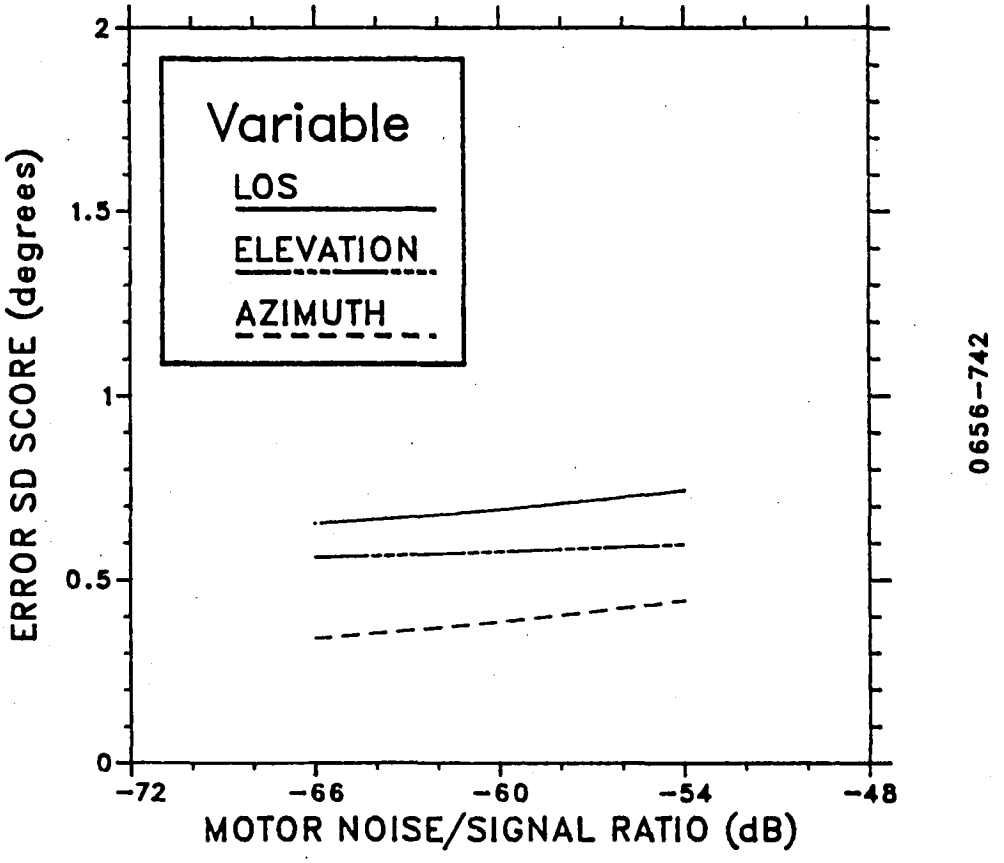

Figure 4.3. Effect of Motor Noise/Signal Ratio on Predicted Error Score

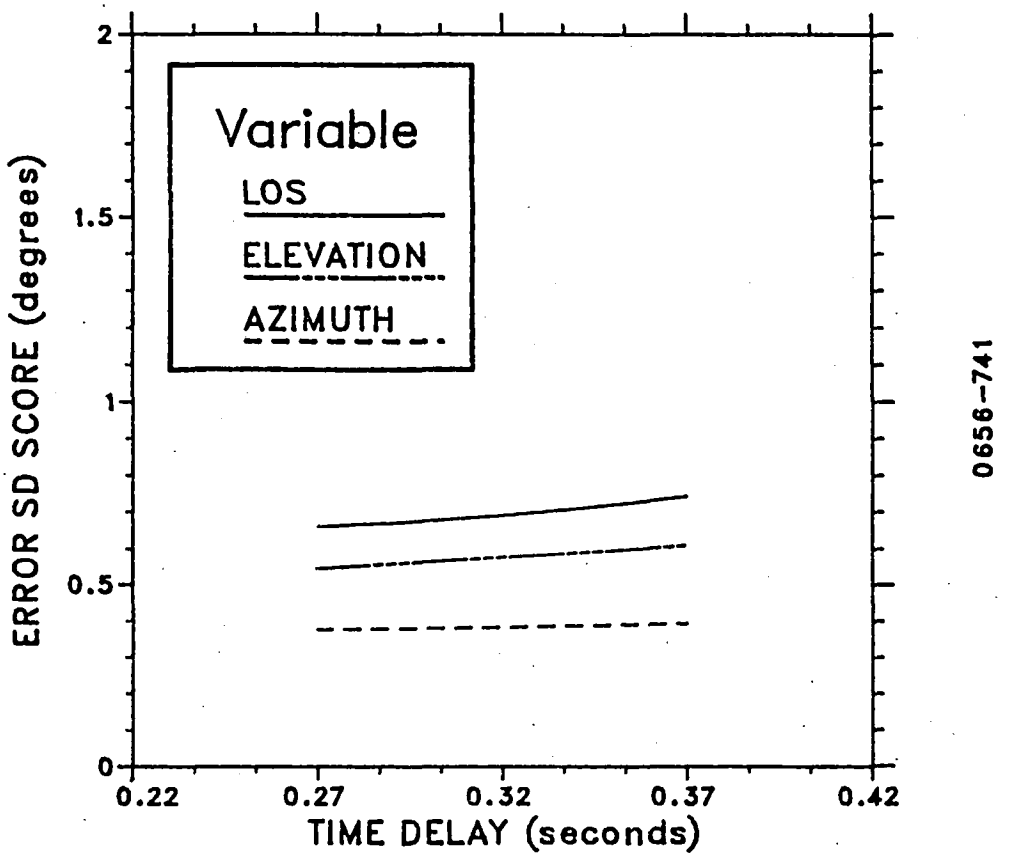

Figure 4.4. Effect of Time Delay on Predicted Error Score

should have little influence on the outcome of the experimental study.

We should note that previous comparisons of model and experimental data indicate that the model may tend to yield optimistic performance predictions when control-loop delays are large. Thus, the sensitivity of actual pilot/vehicle performance to loop delays -- especially for delays on the order of 200 msec and more -- may be greater than that indicated by Figure 4.4.

Potential effects of motion cueing were predicted on the basis of "best-case" assumptions. Specifically, we assumed that platform motion would provide attitude, attitude-rate, and lateral acceleration cues with no attention-sharing penalties, and that perceptual threshold effects for these motion cues would be negligible. Similarly, the g-seat and helmet loader were assumed to provide z-axis acceleration with no degradation. To model the condition with both types of non-visual motion cues present, we adjusted parameters as before and augmented the display vector with all three attitude-rate variables, all three attitude-acceleration variables, along with a_y and n_z; and we assigned unity attentions to all such motion cues.

Performance/workload predictions for the baseline ("visual") case and the visual-motion ("motion") case just described are compared in Figure 4.5. The predicted benefits of non-visual motion cueing are minimal -- less than a 10% improvement in LOS

error at high workload (-20dB observation noise), with this small difference disappearing as observation noise increases.

These predicted trends agree with experimental studies which show that motion cues are most effective when the external forcing function acts directly on the simulated vehicle, and least effective when the external disturbance consists of target maneuvering [12]. These results are also plausible on the basis of a theoretical informational analysis. When the disturbance is applied directly to the vehicle (as, say, a simulated gust disturbance), whole-body and g-seat motion cueing provide the (mathematical) "pilot" directly with vehicle acceleration cues that would not be so readily available from visual cues alone. When there is no external vehicle disturbance, however, vehicle motions are entirely in response to the pilot's control input. In this case, no new information is provided by non-visual motion cueing, and no performance improvement should be expected. The small performance effects shown in Figure 4.5 arise from the inclusion of the motor noise in the model, which prevents the "pilot" from having perfect knowledge of the control input applied to the vehicle.

Arguments can be offered both as to why motion-cue effects should be greater in the simulator (or in flight) than predicted by the model, and why such effects should be less than predicted. On the one hand, we have made very optimistic assumptions

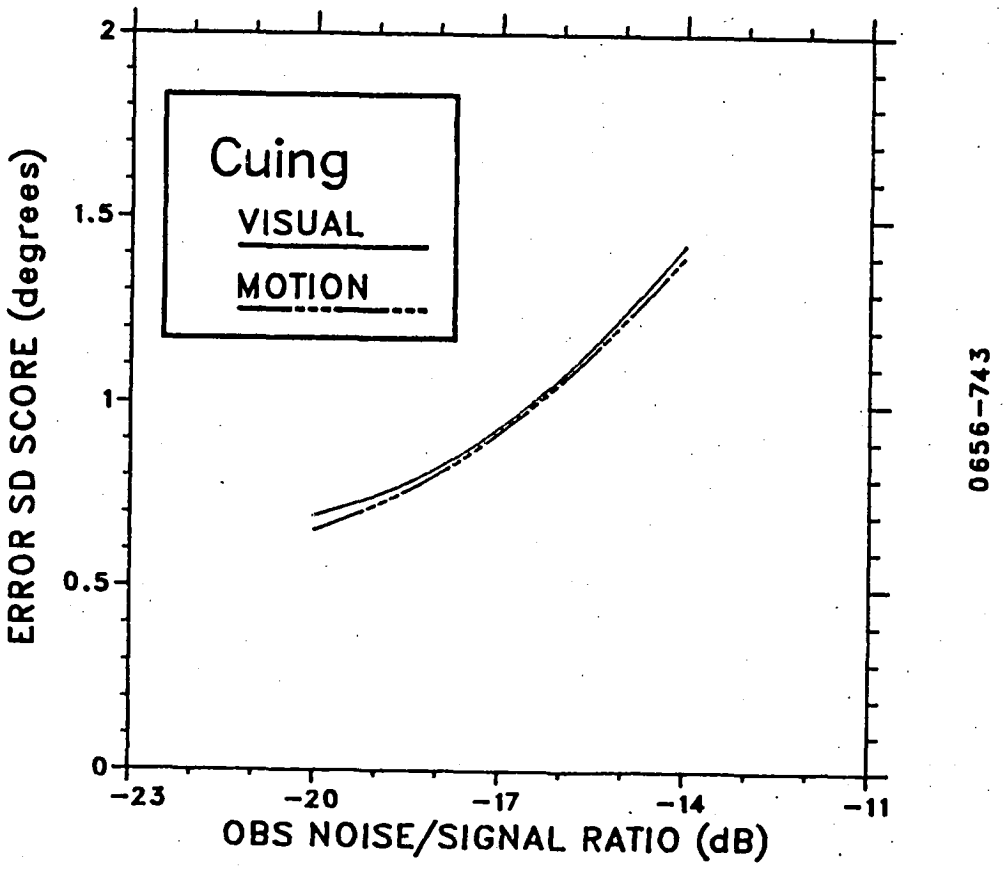

Figure 4.5. Effect of Cueing Environment on Predicted Performance/Workload Tradeoff

concerning the quality of the motion cues received, ignoring perceptual threshold effects, vestibular sensor dynamics, and potential attention-sharing penalties regarding the concurrent use of multiple motion and visual cues. Consideration of these factors would further decrease the visual/motion differences shown in Figure 4.5.

On the other hand, we have made optimistic assumptions concerning the pilot's state of knowledge: namely, that he is trained to the point where he has a near-perfect "internal model" of the vehicle dynamics. To the extent that the pilot is not trained (or trainable) to this state, we expect that visual/motion differences will be greater than predicted, because the motion cues will likely enhance the pilot's ability to construct and maintain an accurate internal plant model [13].

There is some circumstantial, but consistent, evidence to suggest that the accuracy of the pilot's internal model is degraded by insufficient training and/or by the presence of large delays and/or high-order response dynamics in the control loop [13]. The extension of existing pilot models to be able to predict the effects of training and task environment on the pilot's internal model remains as an interesting area of future research.

Recall that the results presented so far were obtained with perceptual "thresholds" selected on the basis of presumed minimum

allowable error ("indifference thresholds") rather than visual resolution limitations. To determine the extent to which predicted line-of-sight errors were tied directly to these threshold parameters, the baseline condition was reanalyzed with parameters adjusted on the basis of visual resolution limitations based on previous tracking results [8]. Thresholds of 0.05 arc degrees were associated with perception of elevation and azimuth error, and rate thresholds were again assumed to be 0.2 deg/sec.

Figure 4.6 shows a substantial reduction in the predicted azimuth error -- about 50% of the rms error predicted with indifference thresholds. The elevation error was reduced by about 30%, and the vector LOS error by about 40%. Clearly, the predicted azimuth error in the baseline case is determined primarily by the selection of a threshold value; this is not surprising, given the lack of a forcing function in the azimuth axis and the relatively low cross-axis coupling provided by system dynamics. The elevation error is less directly dependent on the associated threshold (except for very large thresholds); the predicted error in Figure 4.6 is on the order of 10 times the assumed threshold.

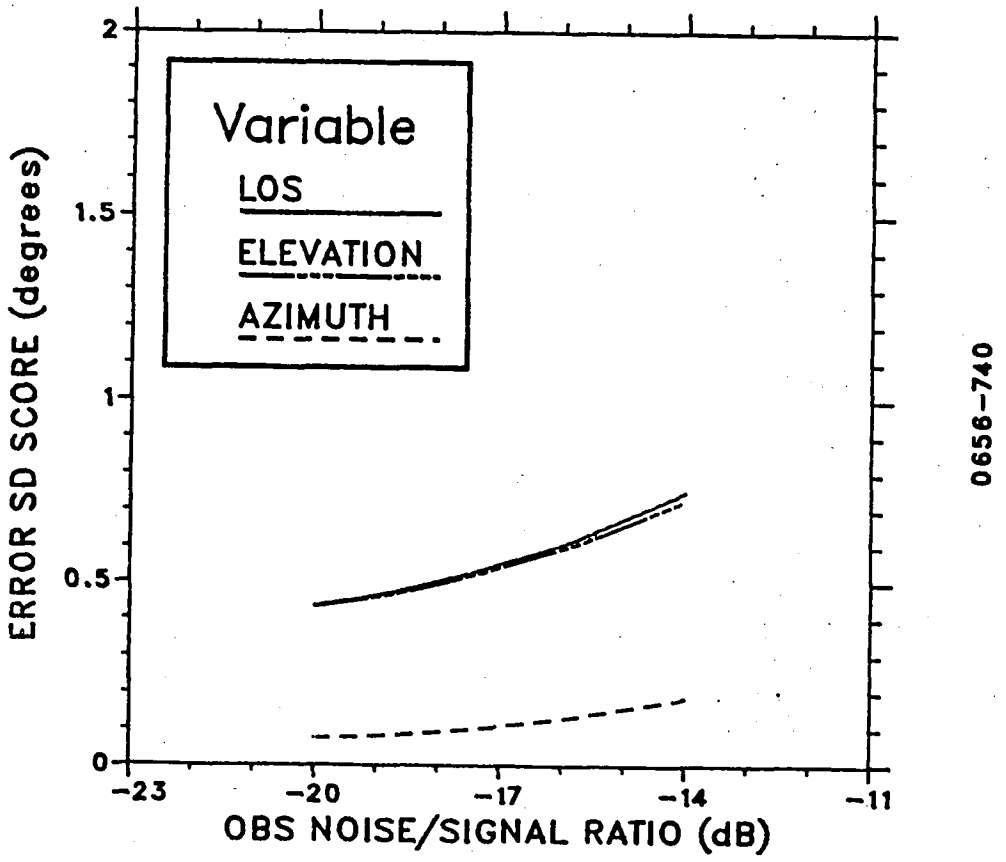

Figure 4.6. Predicted Performance/Workload Tradeoff with Visual Thresholds

5. CONCLUDING REMARKS

The above results represent a preliminary analysis. The most significant portion of our efforts remains; namely, the comparison of model results with the empirical data. Experimental measures and model predictions will include both time domain system performance measures (SD performance scores) and frequency domain measures of pilot-related quantities (describing functions and remnant spectra). Our strategy will be to "tune" the model to each simulator experimental condition by identifying model parameters (time delay, noises, etc.) that provide the "best" match to the data [14]. These parameters, which will also reflect the individual characteristics of the subject pool for the experiment, will then be used to predict results for the flight experiment. Again, model/data comparisons will be made and parameters yielding a best match to the flight data determined. Discrepancies between simulator and flight data will be explored, using the model, to provide analytical bases for the differences in terms of cueing deficiencies and/or changes in pilot strategies and to further upgrade and develop the analytical models.

6. REFERENCES

1. Ashworth, B.R., McKissick, B.T., and Parrish, R.V., "The Effects of Simulation Fidelity on Air-to-Air Tracking", Proc. of Fifteenth Annual Conference on Manual Control, AFFDL-TR-79-3134, Wright Patterson Air Force Base, Ohio, November 1979.

2. Parrish, R.V., McKissick, B.T., and Ashworth, B.R., "The Comparison of Simulator Fidelity Model Predictions with In-Simulator Evaluation Data", NASA TP-2106, February 1983.

3. Baron, S., Muralidharan, R., and Kleinman, D.L., "Closed Loop Models for Analyzing Engineering Requirements for Simulators", NASA CR-2965, February 1980.

4. Kleinman, D.L., Baron, S., and Levison, W.H., "An Optimal Control Model of Human Response", Automatica, Vol. 6, No. 3, pp. 367-384, May 1970.

5. Baron, S., "A Model for Human Control and Monitoring Based on Modern Control Theory", Journal of Cybernetics and Information Science, Vol. 1, No. 1, Spring 1976.

6. Baron, S., "A Multi-Cue OCM for Analysis of Simulator Configurations", Report No. 4373, Bolt Beranek and Newman, Inc., April 1980.

7. Levison, W.H., Elkind, J.I., and Ward, J.L., "Studies of Multivariable Manual Control Systems: A Model for Task Interference", NASA CR-1746, May 1971.

8. Levison, W.H., "The Effects of Display Gain and Signal Bandwidth on Human Controller Remnant", AMRL-TR-70-93, Aerospace Medical Research Laboratory, Wright Patterson Air Force Base, OH, March 1971.

9. Wewerinke, P.H., "Human Operator Workload for Various Control Situations", Tenth Annual Conference on Manual Control, Wright Patterson Air Force Base, OH, 1974.

10. Levison, W.H., "Analysis and In-Simulator Evaluation of Display and Control Concepts for a Terminal Configured Vehicle in Final Approach in a Windshear Environment", NASA CR-3034, August 1978.

11. Baron, S. and Levison, W.H., "Display Analysis with the

Optimal Control Model for the Human Operator", Human Factors, Vol. 19, No. 5, pp. 437-457, October 1977.

12. Levison, W.H. and Junker, A.M., "A Model for the Pilot's Use of Motion Cues in Roll-Axis Tracking Tasks", AMRL-TR-77-40, Aerospace Medical Research Laboratory, June 1977.

13. Levison, W.H., "Development of a Model for Human Operator Learning in Continuous Estimation and Control Tasks", Report No. 5331, Bolt Beranek and Newman, Inc., Cambridge, MA, September 1983.

14. Lancraft, R.E. and Kleinman, D.L., "On the Identification of Parameters in the Optimal Control Model", Proc. of the Fifteenth Annual Conference on Manual Control, Dayton, OH, March 1979.

APPENDIX A
LINEARIZED LINE-OF-SIGHT ERROR EQUATIONS

The elevation line-of-sight (LOS) error, μ, and the azimuth LOS error, λ, are defined as follows:

$$\mu(t) = \frac{Z(t) - Z_1(t)}{D(t)}$$

$$\lambda(t) = \frac{Y_T(t) - Y(t)}{D(t)}$$

where $D(t) = X_T(t) - X(t)$, and where the subscript "T" indicates the position or velocity of the target aircraft in the pursuer's body axis coordinate system. With this sign convention -- which is consistent with the sign convention adopted in the LaRC simulation -- positive LOS error occurs when the target is located above and/or to the right of the projected pursuer's body axis. (Note that positive Z is down.)

Through geometric analysis one arrives at the following expressions for the rate of change of LOS error:

$$\dot{\mu} = \frac{\mu}{D}(U-U_T) + \frac{1}{D}(W-W_T) - Q + P\lambda$$

$$\dot{\lambda} = \frac{\lambda}{D}(U-U_T) - \frac{1}{D}(V-V_T) - R - P\mu$$

If we consider each problem variable to be the sum of steady-state and perturbation terms (e.g., $U = U_o + u$), we arrive at the following expressions for the perturbation in LOS error about the nominal:

$$\dot{\mu} = \frac{\mu_o}{D_o}(\mu-\mu_T) + \frac{1}{D_o}(\omega-\omega_T) + \lambda_o p$$
$$- q + P_o \lambda + p\lambda + \frac{\mu}{D_o}(\mu-\mu_T)$$

$$\dot{\lambda} = \frac{\lambda_o}{D_o}(\mu-\mu_T) - \frac{1}{D_o}(v - v_T) = \mu_o p$$
$$- r - P_o \mu - p\mu + \frac{\lambda}{D}(\mu-\mu_T)$$

The final two terms of each of the above expression represent nonlinearities which, for small perturbations, are not expected to contribute significantly to the LOS error and which will be ignored in the remaining analysis.

APPENDIX B
TARGET KINEMATICS

Note that the equations for LOS error include terms relating to the apparent motion of the target in the pursuer's coordinate frame. In this Appendix we derive the linearized state-variable equations for apparent target motion.

We consider target motion in three different coordinate frames: $\underset{TT}{V}$, the target motion in the (rotating) target coordinate frame, $\underset{TI}{V}$, target motion in some inertial coordinate frame; and $\underset{TP}{V}$, the apparent target motion as seen from the pursuer's (rotating) coordinate frame. Let the translational target velocity components U, V, and W be represented collectively by the vector $\underline{V}$.

Let $\underset{T}{A}$ be the transformation from inertial to pursuer coordinates, and let $\underset{P}{A}$ be the transformation from inertial to pursuer coordinates. Thus:

$$\begin{aligned} \underset{TI}{\underline{V}} &= \underset{T}{\underline{A}}^{-1} \underset{TT}{V} = \underline{A}'\underline{V} \\ \underset{TP}{\underline{V}} &= \underset{P}{\underline{A}}\ \underset{TI}{\underline{V}} = \underset{P}{\underline{A}}\ \underline{A}'\ \underline{V} \end{aligned} \qquad \text{(B.1)}$$

where the prime (') indicates matrix transpose.

Since, for this problem, the target flies a constant circular path, the acceleration of the target in its own coordinate system is zero, and

$$\dot{\underline{V}}_{TP} = [\dot{\underline{A}}_P \, \underline{A}'_T + \underline{A}_P \dot{\underline{A}}'_T] \underline{V}_{TT} \tag{B.2}$$

Note that

$$\dot{\underline{A}} = - \underline{\Omega} \; \underline{A}$$

$$\dot{\underline{A}}' = -\underline{A}' \; \underline{\Omega}' = +\underline{A}' \Omega$$

where

$$\underline{\Omega} = \begin{bmatrix} 0 & -R & -Q \\ \underline{R} & 0 & -P \\ -Q & P & 0 \end{bmatrix} \tag{B.3}$$

Equation A3 may thus be written as:

$$\dot{\underline{V}}_{TP} = [- \underline{\Omega}_P \, \underline{A}_P \, \underline{A}'_T + \underline{A}_P \underline{A}'_T \, \underline{\Omega}_T] V_{TT} \tag{B.4}$$

Because of the coupling between translational and rotational motions, that apparent translational acceleration $\dot{\underline{V}}_{TP}$ will generally be nonzero even though the target has no translational acceleration in its own coordinate frame.

It is convenient to define the inertial coordinate frame as that which overlaps the nominal (i.e., error-free) pursuer coordinate frame at a given time. That is, we take a "snapshot" of the tracking task, align the inertial coordinate frame with the desired position and orientation of the pursuer at that instant, then let the task proceed with the inertial frame fixed in space.

instant, then let the task proceed with the inertial frame fixed in space.

We next define certain problem variables as the sum of their nominal and small-signal-incremental values:

$$\underline{\Omega}_T \equiv \underline{\Omega}_o$$

$$\underline{\Omega}_P = \underline{\Omega}_o + \underline{\omega}$$

$$\underline{\mathbf{A}}_P = \underline{\mathbf{I}} + \underline{\Delta\mathbf{A}}_P \tag{B.5}$$

$$\dot{\underline{V}}_{TP} = \dot{\underline{V}}_{TP_o} + \dot{\underline{v}}_{TP}$$

where Ω_o is the nominal rotation rate of both the target and pursuer. (For this problem, target rotation remains at nominal).

From equations B.4 and B.5 we obtain

$$\dot{\underline{V}}_{TP_o} + \dot{\underline{v}}_{TP} =$$

$$[(-\underline{\Omega}_o + \underline{\omega})(\underline{\mathbf{I}} + \underline{\Delta\mathbf{A}}_P)\underline{\mathbf{A}}'_T + (\underline{\mathbf{I}} + \underline{\Delta\mathbf{A}}_P)\underline{\mathbf{A}}'_T \underline{\Omega}_o]\underline{V}_{TT_o} \tag{B.6}$$

Since steady-state accelerations are zero, $\dot{\underline{V}}_{TP} = \emptyset$, and

$$\underline{\Omega}_o \underline{\mathbf{A}}'_T \underline{V}_{TT_o} = \underline{\mathbf{A}}'_T \underline{\Omega}_o \underline{V}_{TT_o} \tag{B.7}$$

of the pursuer. This acceleration would be apparent even in the case of a straight-and-level tracking task. The terms containing $\Delta\underline{A}_p$ account for apparent translational acceleration due to an off-nominal <u>orientation</u> of the pursuer. This effect scales with the nominal rotation and is therefore zero in a straight-and-level task.

By assuming small deviations of the pursuer's orientation from nominal, we obtain:

$$\Delta\underline{A}_p \approx \begin{bmatrix} 0 & \psi & \theta \\ -\psi & 0 & \phi \\ \theta & -\phi & 0 \end{bmatrix}$$

where $\phi = \int p$, $\theta = \int q$, $\psi = \int r$ (B.9)

Except for nominally straight-and-level tasks, the short-term integrations indicated above will, in general, be different from the Euler angles -- in the case of a high-g turn, substantially different.

From Equations B.3, B.8, and B.9, we obtain the following state-variable equation for the incremental target acceleration as seen in the pursuer's coordinate system:

$$\begin{bmatrix} \dot{u}_{TP} \\ \dot{v}_{TP} \\ \dot{w}_{TP} \end{bmatrix} = \begin{bmatrix} 0 & -W_{TIo} & V_{TIo} & (Q_o V_{TIo} + R_o W_{TIo}) & -P_o V_{TIo} & P_o W_{TIo} \\ W_{TIo} & 0 & -U_{TIo} & -Q_o U_{TIo} & (P_o U_{TIo} + R_o W_{TIo}) & -Q_o W_{TIo} \\ -V_{TIo} & U_{TIo} & 0 & -R_o U_{TIo} & -R_o V_{TIo} & (P_o U_{TIo} + Q_o V_{TIo}) \end{bmatrix} \cdot \begin{bmatrix} p \\ q \\ r \\ \phi \\ \theta \\ \psi \end{bmatrix}$$

(B.10)

The results shown in Equation B.1Ø have been simplified by the particular problem considered in this study, and by our selection of an inertial reference frame. If one were to consider non-steady-state target motion, this expression would have to include the effects of target rotational states. For another choice of inertial reference frame (say, an earth-based reference), the nominal translational velocities U_{TI_o}, etc.) would be replaced by U_{TP_o}, etc. (For the treatment shown here, $\underline{V}_{TI_o} = \underline{V}_{TP_o}$).

The numerical values selected for $\underline{V}_{TI_o}$ in a specific problem depend on the nominal difference in orientation between target and pursuer. For the particular problem explored in this study,

The numerical values selected for $\underline{V}_{TI_o}$ in a specific problem depend on the nominal difference in orientation between target and pursuer. For the particular problem explored in this study, in which the target and nominal pursuer orientations differ only in (earth-based) heading, it is convenient to transform target coordinates to earth-based coordinates and then transform from earth to nominal pursuer coordinates. The parameters used in carrying out this transformation, and the resulting vector velocity $\underline{V}_{TP_o}$, are given in Table B.1.

TABLE B.1 TRANSFORMATION FROM TARGET TO PURSUER COORDINATES

Nominal Orientation:

ϕ_o = -1.23 rad

θ_o = 6.21 E-3 rad

$\Delta\psi_o$ = 0.159 rad

Target Velocity Vector in Target Coordinates:

U_{TT_o} = 686 ft/sec

V_{TT_o} = 5.59 ft/sec

W_{TT_o} = 53.6 ft/sec

Target Velocity Vector in Nominal Pursuer Coordinates:

U_{TI_o} = 686 ft/sec

V_{TI_o} = -30.9 ft/sec

W_{TI_o} = -49.4 ft/sec

APPENDIX C
SYSTEM STATE EQUATIONS

The state-variable equations for the augmented F-14 dynamics, including line-of-sight (LOS) equations and target kinematics, are presented. The state variable description has the form

$$\underline{\dot{x}} = \underline{A}\underline{x} + \underline{B}\underline{u} + \underline{E}\underline{w}$$

$$\underline{y} = \underline{C}\underline{x} + \underline{D}\underline{u}$$

where the vectors $\underline{x}$, $\underline{y}$, $\underline{u}$, and $\underline{w}$ represent system state variables, system output (or display) variables, pilot control inputs, and external driving noise processes.

All equations shown here reflect a linearized model of small-signal deviations about trim conditions.

C.1 Fully-Augmented Aircraft

System dynamics for the fully-augmented F-14 are shown in Figure C.1. Numerical entries for matrices A,B,C, and D are shown, along with a list of system eigenvalues. Effects of pipper motion, which would be represented by the E matrix, are not given here. No external disturbances, other than pilot inputs, were assumed to act on the airplane in this formulation.

To enhance interpretation of the numerical entries, the description of each system matrix includes text information to identify the system variables associated with rows and columns. For example, the row identifiers for the B matrix define system state variables, and the column identifiers define pilot control inputs.

The first eight state variables are standard aircraft response variables as defined in the List of Symbols, the "alt" state represents height deviation from nominal, and variables z1 through z15 are state variables introduced by the augmentation system. The "engine" state represents a first-order lag model of engine response dynamics, "vt" and "wt" are target lateral and vertical motion as seen in the pursuer's coordinate system, and lamda and mu are azimuth and elevation line-of-sight errors.

Many of the state variables also serve as output variables. In addition, the output vector includes acceleration components a_z and a_y, the four aircraft control input (control surfaces, not pilot inputs), and LOS rates of change. The control vector contains the four pilot inputs.

All aircraft translational variables have units of feet, angle variables (including control surfaces) are in radians, and pilot inputs are in inches of control deflection for δ_{ap}, δ_{ep}, and δ_{rp}, and fraction of maximum input for δ_{tp}.

DYNAMICS FOR FULLY-AUGMENTED AIRCRAFT

A MATRIX:

	u	v	w	p	q
	r	theta	phi	alt	z1
	z2	z3	z4	z5	z6
	z14	z8	z9	z15	z11
	z10	z12	z13	engine	vt
	wt	lambda	mu		
u	-3.750E-02	-4.860E-02	-3.220E-02	0.	-5.220E+01
	5.590E+00	-3.220E+01	0.	-1.380E-05	0.
	0.	0.	0.	0.	0.
	6.440E-02	0.	0.	0.	0.
	0.	0.	0.	6.130E-04	0.
	0.	0.	0.		
v	3.260E-02	-2.000E-01	9.270E-03	5.500E+01	0.
	-6.820E+02	1.890E-01	1.070E+01	-3.420E-05	0.
	0.	0.	0.	0.	0.
	0.	0.	0.	1.610E-01	0.
	0.	0.	7.080E-01	0.	0.
	0.	0.	0.		
w	-4.500E-02	-5.510E-02	-1.210E+00	-5.590E+00	6.770E+02
	0.	-6.670E-02	3.040E+01	3.050E-03	0.
	0.	0.	0.	0.	0.
	-9.790E-01	0.	0.	0.	0.
	0.	0.	0.	7.490E-06	0.
	0.	0.	0.		
p	-3.080E-05	-3.090E-02	-1.270E-03	-4.650E+00	3.860E-02
	5.300E-01	0.	0.	-8.970E-07	0.
	0.	0.	0.	0.	0.
	0.	0.	0.	-2.260E-01	0.
	0.	0.	3.690E-02	0.	0.
	0.	0.	0.		
q	1.950E-03	-4.800E-04	-1.710E-03	-4.300E-02	-1.120E+00
	1.480E-03	0.	0.	6.060E-06	0.
	0.	0.	0.	0.	0.
	-9.790E-02	0.	0.	0.	0.
	0.	0.	0.	3.590E-06	0.
	0.	0.	0.		
r	-1.050E-04	7.460E-03	-4.300E-05	-2.610E-01	-1.110E-03
	-3.050E-01	0.	0.	-7.640E-08	0.
	0.	0.	0.	0.	0.
	0.	0.	0.	-2.350E-02	0.
	0.	0.	-6.970E-02	0.	0.
	0.	0.	0.		
theta	0.	0.	0.	0.	3.330E-01
	9.430E-01	0.	1.320E-01	0.	0.
	0.	0.	0.	0.	0.
	0.	0.	0.	0.	0.
	0.	0.	0.	0.	0.
	0.	0.	0.		

FIG. C.1 SYSTEM DYNAMICS USED FOR PILOT/VEHICLE MODEL ANALYSIS

phi	0.	0.	0.	1.000E+00	-5.860E-03
	2.070E-03	-1.320E-01	0.	0.	0.
	0.	0.	0.	0.	0.
	0.	0.	0.	0.	0.
	0.	0.	0.	0.	0.
	0.	0.	0.		
alt	6.210E-03	9.430E-01	-3.330E-01	0.	0.
	0.	6.860E+02	-5.240E+01	0.	0.
	0.	0.	0.	0.	0.
	0.	0.	0.	0.	0.
	0.	0.	0.	0.	0.
	0.	0.	0.		
z1	0.	0.	0.	0.	2.860E+01
	0.	0.	0.	0.	-5.000E-01
	0.	0.	0.	0.	0.
	0.	0.	0.	0.	0.
	0.	0.	0.	0.	0.
	0.	0.	0.		
z2	0.	0.	0.	0.	1.080E+02
	0.	0.	0.	0.	-1.890E+00
	-1.890E+00	0.	0.	0.	0.
	0.	0.	0.	0.	0.
	0.	0.	0.	0.	0.
	0.	0.	0.		
z3	0.	0.	0.	0.	1.080E+02
	0.	0.	0.	0.	-1.890E+00
	0.	-1.890E+00	0.	0.	0.
	0.	0.	0.	0.	0.
	0.	0.	0.	0.	0.
	0.	0.	0.		
z4	0.	0.	0.	0.	3.020E+02
	0.	0.	0.	0.	-5.280E+00
	-5.280E+00	1.400E+01	-1.400E+01	0.	0.
	0.	0.	0.	0.	0.
	0.	0.	0.	0.	0.
	0.	0.	0.		
z5	0.	0.	0.	0.	3.020E+02
	0.	0.	0.	0.	-5.280E+00
	-5.280E+00	1.400E+01	0.	-1.400E+01	0.
	0.	0.	0.	0.	0.
	0.	0.	0.	0.	0.
	0.	0.	0.		
z6	0.	0.	0.	0.	4.030E+03
	0.	0.	0.	0.	-7.040E+01
	-7.040E+01	1.860E+02	-1.860E+02	6.670E+01	-6.670E+01
	0.	0.	0.	0.	0.
	0.	0.	0.	0.	0.
	0.	0.	0.		
z14	0.	0.	0.	0.	0.
	0.	0.	0.	0.	0.
	0.	0.	0.	0.	1.200E+01

FIG. C.1 (Continued)

	-2.000E+01	0.	0.	0.	0.
	0.	0.	0.	0.	0.
	0.	0.	0.		
z8	0.	0.	0.	0.	0.
	0.	0.	0.	0.	0.
	0.	0.	0.	0.	0.
	0.	-2.000E+00	0.	0.	0.
	0.	0.	0.	0.	0.
	0.	0.	0.		
z9	0.	0.	0.	2.063E+02	0.
	0.	0.	0.	0.	0.
	0.	0.	0.	0.	0.
	0.	-9.000E+01	-9.000E+01	0.	0.
	0.	0.	0.	0.	0.
	0.	0.	0.		
z15	0.	0.	0.	0.	0.
	0.	0.	0.	0.	0.
	0.	0.	0.	0.	0.
	0.	0.	4.000E+01	-2.000E+01	0.
	0.	0.	0.	0.	0.
	0.	0.	0.		
z11	-6.560E-02	-1.130E+00	4.800E-02	8.160E+00	0.
	2.200E+01	0.	0.	-1.940E-04	0.
	0.	0.	0.	0.	0.
	0.	0.	0.	9.120E-01	-2.000E+01
	0.	0.	4.020E+00	0.	0.
	0.	0.	0.		
z10	0.	0.	0.	0.	0.
	2.860E+01	0.	0.	0.	0.
	0.	0.	0.	0.	0.
	0.	0.	0.	0.	0.
	-5.000E-01	0.	0.	0.	0.
	0.	0.	0.		
z12	0.	0.	0.	0.	0.
	5.160E+03	0.	0.	0.	0.
	0.	0.	0.	0.	0.
	0.	0.	0.	0.	9.000E+01
	-9.000E+01	-9.000E+01	0.	0.	0.
	0.	0.	0.		
z13	0.	0.	0.	0.	0.
	0.	0.	0.	0.	0.
	0.	0.	0.	0.	0.
	0.	0.	0.	0.	0.
	0.	2.000E+01	-2.000E+01	0.	0.
	0.	0.	0.		
engine	2.020E+00	1.650E-02	1.580E-01	0.	0.
	0.	0.	0.	-2.170E-01	0.
	0.	0.	0.	0.	0.
	0.	0.	0.	0.	0.
	0.	0.	0.	-5.000E-01	0.
	0.	0.	0.		

FIG. C.1 (Continued)

vt	0.	0.	0.	-5.200E+01	0.
	-6.850E+02	0.	-8.560E+01	0.	0.
	0.	0.	0.	0.	0.
	0.	0.	0.	0.	0.
	0.	0.	0.	0.	0.
	0.	0.	0.		
wt	0.	0.	0.	3.190E+01	6.850E+02
	0.	0.	3.020E+01	0.	0.
	0.	0.	0.	0.	0.
	0.	0.	0.	0.	0.
	0.	0.	0.	0.	0.
	0.	0.	0.		
lambda	-5.610E-06	-1.190E-03	0.	9.260E-02	0.
	-1.000E+00	0.	0.	0.	0.
	0.	0.	0.	0.	0.
	0.	0.	0.	0.	0.
	0.	0.	0.	0.	1.190E-03
	0.	0.	-8.240E-04		
mu	-1.100E-04	0.	1.190E-03	-4.720E-03	-1.000E+00
	0.	0.	0.	0.	0.
	0.	0.	0.	0.	0.
	0.	0.	0.	0.	0.
	0.	0.	0.	0.	0.
	-1.190E-03	8.240E-04	0.		

B MATRIX:

	delta-ep	delta-ap	delta-rp	delta-tp
u	0.	0.	0.	0.
v	0.	0.	0.	0.
w	0.	0.	0.	0.
p	0.	0.	0.	0.
q	0.	0.	0.	0.
r	0.	0.	0.	0.
theta	0.	0.	0.	0.
phi	0.	0.	0.	0.
alt	0.	0.	0.	0.
z1	0.	0.	0.	0.
z2	0.	0.	0.	0.
z3	0.	0.	0.	0.
z4	0.	0.	0.	0.
z5	0.	0.	0.	0.
z6	0.	0.	0.	0.
z14	-1.080E+02	0.	0.	0.
z8	0.	8.560E+00	0.	0.
z9	0.	0.	0.	0.
z15	0.	-8.000E+01	0.	0.
z11	0.	0.	0.	0.
z10	0.	0.	0.	0.
z12	0.	0.	0.	0.
z13	0.	0.	-2.000E+02	0.
engine	0.	0.	0.	1.430E+04
vt	0.	0.	0.	0.
wt	0.	0.	0.	0.
lambda	0.	0.	0.	0.
mu	0.	0.	0.	0.

FIG. C.1 (Continued)

NO NOISE INPUTS

C MATRIX:

	u	v	w	p	q
	r	theta	phi	alt	z1
	z2	z3	z4	z5	z6
	z14	z8	z9	z15	z11
	z10	z12	z13	engine	vt
	wt	lambda	mu		
u	1.000E+00	0.	0.	0.	0.
	0.	0.	0.	0.	0.
	0.	0.	0.	0.	0.
	0.	0.	0.	0.	0.
	0.	0.	0.	0.	0.
	0.	0.	0.		
v	0.	1.000E+00	0.	0.	0.
	0.	0.	0.	0.	0.
	0.	0.	0.	0.	0.
	0.	0.	0.	0.	0.
	0.	0.	0.	0.	0.
	0.	0.	0.		
w	0.	0.	1.000E+00	0.	0.
	0.	0.	0.	0.	0.
	0.	0.	0.	0.	0.
	0.	0.	0.	0.	0.
	0.	0.	0.	0.	0.
	0.	0.	0.		
p	0.	0.	0.	1.000E+00	0.
	0.	0.	0.	0.	0.
	0.	0.	0.	0.	0.
	0.	0.	0.	0.	0.
	0.	0.	0.	0.	0.
	0.	0.	0.		
q	0.	0.	0.	0.	1.000E+00
	0.	0.	0.	0.	0.
	0.	0.	0.	0.	0.
	0.	0.	0.	0.	0.
	0.	0.	0.	0.	0.
	0.	0.	0.		
r	0.	0.	0.	0.	0.
	1.000E+00	0.	0.	0.	0.
	0.	0.	0.	0.	0.
	0.	0.	0.	0.	0.
	0.	0.	0.	0.	0.
	0.	0.	0.		
theta	0.	0.	0.	0.	0.
	0.	1.000E+00	0.	0.	0.
	0.	0.	0.	0.	0.
	0.	0.	0.	0.	0.
	0.	0.	0.	0.	0.
	0.	0.	0.		

FIG. C.1 (Continued)

phi	0.	0.	0.	0.	0.
	0.	0.	1.000E+00	0.	0.
	0.	0.	0.	0.	0.
	0.	0.	0.	0.	0.
	0.	0.	0.	0.	0.
	0.	0.	0.		
alt	0.	0.	0.	0.	0.
	0.	0.	0.	1.000E+00	0.
	0.	0.	0.	0.	0.
	0.	0.	0.	0.	0.
	0.	0.	0.	0.	0.
	0.	0.	0.		
az	4.500E-02	5.510E-02	1.210E+00	5.590E+00	5.000E+00
	0.	6.670E-02	-3.040E+01	-3.050E-03	0.
	0.	0.	0.	0.	0.
	9.790E-01	0.	0.	0.	0.
	0.	0.	0.	-7.490E-06	0.
	0.	0.	0.		
ay	-3.280E-03	-5.650E-02	2.400E-03	4.080E-01	0.
	1.100E+00	0.	0.	-9.700E-06	0.
	0.	0.	0.	0.	0.
	0.	0.	0.	4.560E-02	0.
	0.	0.	2.010E-01	0.	0.
	0.	0.	0.		
delta-e	0.	0.	0.	0.	0.
	0.	0.	0.	0.	0.
	0.	0.	0.	0.	0.
	1.000E+00	0.	0.	0.	0.
	0.	0.	0.	0.	0.
	0.	0.	0.		
delta-a	0.	0.	0.	0.	0.
	0.	0.	0.	0.	0.
	0.	0.	0.	0.	0.
	0.	0.	0.	1.000E+00	0.
	0.	0.	0.	0.	0.
	0.	0.	0.		
delta-r	0.	0.	0.	0.	0.
	0.	0.	0.	0.	0.
	0.	0.	0.	0.	0.
	0.	0.	0.	0.	0.
	0.	0.	1.000E+00	0.	0.
	0.	0.	0.		
delta-t	0.	0.	0.	0.	0.
	0.	0.	0.	0.	0.
	0.	0.	0.	0.	0.
	0.	0.	0.	0.	0.
	0.	0.	0.	1.000E+00	0.
	0.	0.	0.		
vt	0.	0.	0.	0.	0.
	0.	0.	0.	0.	0.
	0.	0.	0.	0.	0.
	0.	0.	0.	0.	0.

FIG. C.1 (Continued)

	0.	0.	0.	0.	1.000E+00
	0.	0.	0.		
wt	0.	0.	0.	0.	0.
	0.	0.	0.	0.	0.
	0.	0.	0.	0.	0.
	0.	0.	0.	0.	0.
	0.	0.	0.	0.	0.
	1.000E+00	0.	0.		
lambda	0.	0.	0.	0.	0.
	0.	0.	0.	0.	0.
	0.	0.	0.	0.	0.
	0.	0.	0.	0.	0.
	0.	0.	0.	0.	0.
	0.	1.000E+00	0.		
mu	0.	0.	0.	0.	0.
	0.	0.	0.	0.	0.
	0.	0.	0.	0.	0.
	0.	0.	0.	0.	0.
	0.	0.	0.	0.	0.
	0.	0.	1.000E+00		
lambda dot	-5.610E-06	-1.190E-03	0.	9.260E-02	0.
	-1.000E+00	0.	0.	0.	0.
	0.	0.	0.	0.	0.
	0.	0.	0.	0.	0.
	0.	0.	0.	0.	1.190E-03
	0.	0.	-8.240E-04		
mu dot	-1.100E-04	0.	1.190E-03	-4.720E-03	-1.000E+00
	0.	0.	0.	0.	0.
	0.	0.	0.	0.	0.
	0.	0.	0.	0.	0.
	0.	0.	0.	0.	0.
	-1.190E-03	8.240E-04	0.		

D MATRIX:

	delta-ep	delta-ap	delta-rp	delta-tp
u	0.	0.	0.	0.
v	0.	0.	0.	0.
w	0.	0.	0.	0.
p	0.	0.	0.	0.
q	0.	0.	0.	0.
r	0.	0.	0.	0.
theta	0.	0.	0.	0.
phi	0.	0.	0.	0.
alt	0.	0.	0.	0.
az	0.	0.	0.	0.
ay	0.	0.	0.	0.
delta-e	0.	0.	0.	0.
delta-a	0.	0.	0.	0.
delta-r	0.	0.	0.	0.
delta-t	0.	0.	0.	0.
vt	0.	0.	0.	0.
wt	0.	0.	0.	0.
lambda	0.	0.	0.	0.
mu	0.	0.	0.	0.

FIG. C.1 (Continued)

lambda dot	0.	0.	0.	0.
mu dot	0.	0.	0.	0.

EIGENVALUES

	REAL	IMAG	FREQ	DMPG
1	-6.833E+01	0.000E+00	6.833E+01	1.000E+00
2	-8.967E+01	0.000E+00	8.967E+01	1.000E+00
3	-9.031E+01	0.000E+00	9.031E+01	1.000E+00
4	-2.904E+01	0.000E+00	2.904E+01	1.000E+00
5	-1.539E+01	7.068E+00	1.694E+01	9.088E-01
6	-1.539E+01	-7.068E+00	1.694E+01	9.088E-01
7	-1.797E+01	0.000E+00	1.797E+01	1.000E+00
8	-4.662E+00	4.734E+00	6.644E+00	7.017E-01
9	-4.662E+00	-4.734E+00	6.644E+00	7.017E-01
10	-6.549E+00	0.000E+00	6.549E+00	1.000E+00
11	-1.400E+01	0.000E+00	1.400E+01	1.000E+00
12	-2.403E+00	1.897E+00	3.061E+00	7.849E-01
13	-2.403E+00	-1.897E+00	3.061E+00	7.849E-01
14	-2.216E+00	0.000E+00	2.216E+00	1.000E+00
15	-1.283E+00	0.000E+00	1.283E+00	1.000E+00
16	-5.027E-01	0.000E+00	5.027E-01	1.000E+00
17	-5.869E-01	0.000E+00	5.869E-01	1.000E+00
18	-1.890E+00	0.000E+00	1.890E+00	1.000E+00
19	-1.150E-02	1.664E-01	1.668E-01	6.894E-02
20	-1.150E-02	-1.664E-01	1.668E-01	6.894E-02
21	-1.662E-01	0.000E+00	1.662E-01	1.000E+00
22	-2.000E+00	0.000E+00	2.000E+00	1.000E+00
23	-6.151E-02	0.000E+00	6.151E-02	1.000E+00
24	-8.217E-04	3.040E-03	3.149E-03	2.609E-01
25	-8.217E-04	-3.040E-03	3.149E-03	2.609E-01
26	3.344E-06	8.242E-04	8.242E-04	-4.058E-03
27	3.344E-06	-8.242E-04	8.242E-04	-4.058E-03
28	-9.226E-05	0.000E+00	9.226E-05	1.000E+00

FIG. C.1 (Concluded)

C.2 Aircraft with Reduced-Order Augmentation

Figure C.2 contains system matrices for the reduced-order augmentation. The reader will notice that many of the state variables have been eliminated. In particular, the augmentation system is reduced to three states, with one state each for the pitch, roll, and yaw axis augmentation systems. Output and control variables are the same as for the fully augmented aircraft.

lambda	-5.610E-06	-1.190E-03	0.	9.260E-02	0.
	-1.000E+00	0.	0.	0.	0.
	0.	1.190E-03	0.	0.	-8.240E-04
mu	-1.100E-04	0.	1.190E-03	-4.720E-03	-1.000E+00
	0.	0.	0.	0.	0.
	0.	0.	-1.190E-03	8.240E-04	0.

B MATRIX:

	delta-ep	delta-ap	delta-rp	delta-tp
u	-3.458E-01	0.	0.	1.753E+01
v	0.	-3.182E-01	-8.861E+00	0.
w	5.257E+00	0.	0.	2.142E-01
p	0.	3.538E-01	-4.618E-01	0.
q	5.257E-01	0.	0.	1.027E-01
r	0.	4.342E-02	8.723E-01	0.
theta	0.	0.	0.	0.
phi	0.	0.	0.	0.
pit1	0.	0.	0.	0.
rol1	0.	-1.580E+00	0.	0.
yaw1	0.	0.	0.	0.
vt	0.	0.	0.	0.
wt	0.	0.	0.	0.
lambda	0.	0.	0.	0.
mu	0.	0.	0.	0.

NO NOISE INPUTS

C MATRIX:

	u r yaw1	v theta vt	w phi wt	p pit1 lambda	q rol1 mu
u	1.000E+00	0.	0.	0.	0.
	0.	0.	0.	0.	0.
	0.	0.	0.	0.	0.
v	0.	1.000E+00	0.	0.	0.
	0.	0.	0.	0.	0.
	0.	0.	0.	0.	0.
w	0.	0.	1.000E+00	0.	0.
	0.	0.	0.	0.	0.
	0.	0.	0.	0.	0.
p	0.	0.	0.	1.000E+00	0.
	0.	0.	0.	0.	0.
	0.	0.	0.	0.	0.
q	0.	0.	0.	0.	1.000E+00
	0.	0.	0.	0.	0.
	0.	0.	0.	0.	0.
r	0.	0.	0.	0.	0.
	1.000E+00	0.	0.	0.	0.
	0.	0.	0.	0.	0.

FIG. C.2 (Continued)

theta	0.	0.	0.	0.	0.
	0.	1.000E+00	0.	0.	0.
	0.	0.	0.	0.	0.
phi	0.	0.	0.	0.	0.
	0.	0.	1.000E+00	0.	0.
	0.	0.	0.	0.	0.
alt	0.	0.	0.	0.	0.
	0.	0.	0.	0.	0.
	0.	0.	0.	0.	0.
az	4.497E-02	5.510E-02	1.210E+00	5.590E+00	2.879E+01
	0.	6.670E-02	-3.040E+01	2.379E+01	0.
	0.	0.	0.	0.	0.
ay	-4.105E-03	-7.071E-02	3.004E-03	7.715E-01	0.
	1.456E+01	0.	0.	0.	1.079E+00
	1.318E+01	0.	0.	0.	0.
delta-e	0.	0.	0.	0.	2.430E+01
	0.	0.	0.	2.430E+01	0.
	0.	0.	0.	0.	0.
delta-a	0.	0.	0.	4.570E+00	0.
	0.	0.	0.	0.	1.890E+01
	0.	0.	0.	0.	0.
delta-r	-4.105E-03	-7.071E-02	3.004E-03	7.715E-01	0.
	6.696E+01	0.	0.	0.	1.079E+00
	6.558E+01	0.	0.	0.	0.
delta-t	4.040E+00	3.300E-02	3.160E-01	0.	0.
	0.	0.	0.	0.	0.
	0.	0.	0.	0.	0.
vt	0.	0.	0.	0.	0.
	0.	0.	0.	0.	0.
	0.	1.000E+00	0.	0.	0.
wt	0.	0.	0.	0.	0.
	0.	0.	0.	0.	0.
	0.	0.	1.000E+00	0.	0.
lambda	0.	0.	0.	0.	0.
	0.	0.	0.	0.	0.
	0.	0.	0.	1.000E+00	0.
mu	0.	0.	0.	0.	0.
	0.	0.	0.	0.	0.
	0.	0.	0.	0.	1.000E+00
lambda dot	-5.610E-06	-1.190E-03	0.	9.260E-02	0.
	-1.000E+00	0.	0.	0.	0.
	0.	1.190E-03	0.	0.	-8.240E-04
mu dot	-1.100E-04	0.	1.190E-03	-4.720E-03	-1.000E+00
	0.	0.	0.	0.	0.
	0.	0.	-1.190E-03	8.240E-04	0.

FIG. C.2 (Continued)

D MATRIX

	delta-ep	delta-ap	delta-rp	delta-tp
u	0.	0.	0.	0.
v	0.	0.	0.	0.
w	0.	0.	0.	0.
p	0.	0.	0.	0.
q	0.	0.	0.	0.
r	0.	0.	0.	0.
theta	0.	0.	0.	0.
phi	0.	0.	0.	0.
alt	0.	0.	0.	0.
az	-5.257E+00	0.	0.	-2.142E-01
ay	0.	-9.017E-02	-2.516E+00	0.
delta-e	-5.370E+00	0.	0.	0.
delta-a	0.	-1.580E+00	0.	0.
delta-r	0.	-9.017E-02	-1.252E+01	0.
delta-t	0.	0.	0.	2.860E+04
vt	0.	0.	0.	0.
wt	0.	0.	0.	0.
lambda	0.	0.	0.	0.
mu	0.	0.	0.	0.
lambda dot	0.	0.	0.	0.
mu dot	0.	0.	0.	0.

EIGENVALUES

	REAL	IMAG	FREQ	DMPG
1	-5.563E+00	0.000E+00	5.563E+00	1.000E+00
2	-2.634E+00	1.771E+00	3.174E+00	8.299E-01
3	-2.634E+00	-1.771E+00	3.174E+00	8.299E-01
4	-3.189E+00	0.000E+00	3.189E+00	1.000E+00
5	-1.658E+00	0.000E+00	1.658E+00	1.000E+00
6	-4.632E-01	0.000E+00	4.632E-01	1.000E+00
7	-1.324E-02	1.662E-01	1.667E-01	7.942E-02
8	-1.324E-02	-1.662E-01	1.667E-01	7.942E-02
9	-1.364E-01	0.000E+00	1.364E-01	1.000E+00
10	-5.809E-02	0.000E+00	5.809E-02	1.000E+00
11	-2.845E-06	7.727E-04	7.727E-04	3.682E-03
12	-2.845E-06	-7.727E-04	7.727E-04	3.682E-03
13	-2.810E+00	0.000E+00	2.810E+00	1.000E+00
14	1.333E-05	1.026E-06	1.337E-05	-9.971E-01
15	1.333E-05	-1.026E-06	1.337E-05	-9.971E-01

FIG. C.2 (Concluded)

C.3 System Dynamics Used for Pilot Modeling

The system matrices used for predictions of closed-loop pilot/vehicle performance are presented in Figure C.3. These dynamics differ from the dynamics described above as follows:

- All angle variables are in degrees.
- The states "pip1" and "pip2" representing pipper motion are included.
- Only two pilot inputs are included: δ_e and δ_a.
- altitude has been removed as an output variable, and four new outputs are included: mu error and mu error rate, representing the difference between the vertical pipper displacement or rate and the position or rate of the LOS to the target (i.e., the vertical-axis tracking error); and the displacement and rate of the pipper with respect to its nominal position within the HUD.
- Airspeed is retained as an output, but has zero value because of the removal of the airspeed state variable.

When computing pilot response strategy, the OCM temporarily reduced the output vector to contain only those variables used by the pilot (a small subset of the output vector represented in Figure C.3.). Once a model solution was obtained, the full output vector was restored for the purposes of computing output variance scores.

SYSTEM DYNAMICS USED FOR PILOT MODELING

TOTAL NO. NOISE STATES = 2

A MATRIX:

	pip1 q roll mu	pip2 r yaw1	v theta vt	w phi wt	p pit1 lambda
pip1	-2.500E-01	0.	0.	0.	0.
	0.	0.	0.	0.	0.
	0.	0.	0.	0.	0.
	0.				
pip2	1.000E+00	-5.000E-01	0.	0.	0.
	0.	0.	0.	0.	0.
	0.	0.	0.	0.	0.
	0.				
v	0.	0.	-2.501E-01	1.140E-02	5.628E+01
	0.	-6.346E+02	1.890E-01	1.070E+01	0.
	3.807E+00	4.643E+01	0.	0.	0.
	0.				
w	0.	0.	-5.510E-02	-1.210E+00	-5.590E+00
	6.532E+02	0.	-6.670E-02	3.040E+01	-2.379E+01
	0.	0.	0.	0.	0.
	0.				
p	0.	0.	-3.351E-02	-1.159E-03	-5.654E+00
	3.860E-02	3.001E+00	0.	0.	0.
	-4.232E+00	2.420E+00	0.	0.	0.
	0.				
q	0.	0.	-4.799E-04	-1.709E-03	-4.300E-02
	-3.499E+00	1.480E-03	0.	0.	-2.379E+00
	0.	0.	0.	0.	0.
	0.				
r	0.	0.	1.239E-02	-2.524E-04	-4.222E-01
	-1.110E-03	-4.972E+00	0.	0.	0.
	-5.193E-01	-4.571E+00	0.	0.	0.
	0.				
theta	0.	0.	0.	0.	0.
	3.330E-01	9.430E-01	0.	1.320E-01	0.
	0.	0.	0.	0.	0.
	0.				
phi	0.	0.	0.	0.	1.000E+00
	-5.860E-03	2.070E-03	-1.320E-01	0.	0.
	0.	0.	0.	0.	0.
	0.				
pit1	0.	0.	0.	0.	0.
	-3.180E-01	0.	0.	0.	-3.180E-01
	0.	0.	0.	0.	0.

FIG. C.3 SYSTEM DYNAMICS FOR AIRCRAFT WITH REDUCED-ORDER AUGMENTATION

	0.				
roll	0.	0.	0.	0.	0.
	0.	0.	0.	0.	0.
	-2.810E+00	0.	0.	0.	0.
	0.				
yawl	0.	0.	0.	0.	0.
	0.	-4.240E-01	0.	0.	0.
	0.	-4.240E-01	0.	0.	0.
	0.				
vt	0.	0.	0.	0.	-5.200E+01
	0.	-6.850E+02	0.	-8.560E+01	0.
	0.	0.	0.	0.	0.
	0.				
wt	0.	0.	0.	0.	3.190E+01
	6.850E+02	0.	0.	3.020E+01	0.
	0.	0.	0.	0.	0.
	0.				
lambda	0.	0.	-1.190E-03	0.	9.260E-02
	0.	-1.000E+00	0.	0.	0.
	0.	0.	1.190E-03	0.	0.
	-8.240E-04				
mu	0.	0.	0.	1.190E-03	-4.720E-03
	-1.000E+00	0.	0.	0.	0.
	0.	0.	0.	-1.190E-03	8.240E-04
	0.				

B MATRIX.

	delta-ep	delta-ap
pipl	0.	0.
pip2	0.	0.
v	0.	-3.182E-01
w	5.257E+00	0.
p	0.	3.538E-01
q	5.257E-01	0.
r	0.	4.342E-02
theta	0.	0.
phi	0.	0.
pitl	0.	0.
roll	0.	-1.580E+00
yawl	0.	0.
vt	0.	0.
wt	0.	0.
lambda	0.	0.
mu	0.	0.

E MATRIX:

	noise
pipl	4.330E-01
pip2	0.
v	0.
w	0.
p	0.

FIG. C.3 (Continued)

q	0.
r	0.
theta	0.
phi	0.
pit1	0.
rol1	0.
yaw1	0.
vt	0.
wt	0.
lambda	0.
mu	0.

C MATRIX:

	pip1 q rol1 mu	pip2 r yaw1	v theta vt	w phi wt	p pit1 lambda
u	0. 0. 0. 0.	0. 0. 0.	0. 0. 0.	0. 0. 0.	0. 0. 0.
v	0. 0. 0. 0.	0. 0. 0.	1.000E+00 0. 0.	0. 0. 0.	0. 0. 0.
w	0. 0. 0. 0.	0. 0. 0.	0. 0. 0.	1.000E+00 0. 0.	0. 0. 0.
p	0. 0. 0. 0.	0. 0. 0.	0. 0. 0.	0. 0. 0.	5.730E+01 0. 0.
q	0. 5.730E+01 0. 0.	0. 0. 0.	0. 0. 0.	0. 0. 0.	0. 0. 0.
r	0. 0. 0. 0.	0. 5.730E+01 0.	0. 0. 0.	0. 0. 0.	0. 0. 0.
theta	0. 0. 0. 0.	0. 0. 0.	0. 5.730E+01 0.	0. 0. 0.	0. 0. 0.
phi	0. 0. 0. 0.	0. 0. 0.	0. 0. 0.	0. 5.730E+01 0.	0. 0. 0.
az	0. 2.879E+01	0. 0.	5.510E-02 6.670E-02	1.210E+00 -3.040E+01	5.590E+00 2.379E+01

FIG. C.3 (Continued)

	0.	0.	0.	0.	0.
	0.				
ay	0.	0.	-7.071E-02	3.004E-03	7.715E-01
	0.	1.456E+01	0.	0.	0.
	1.079E+00	1.318E+01	0.	0.	0.
	0.				
delta-e	0.	0.	0.	0.	0.
	2.430E+01	0.	0.	0.	2.430E+01
	0.	0.	0.	0.	0.
	0.				
delta-a	0.	0.	0.	0.	4.570E+00
	0.	0.	0.	0.	0.
	1.890E+01	0.	0.	0.	0.
	0.				
delta-r	0.	0.	-7.071E-02	3.004E-03	7.715E-01
	0.	6.696E+01	0.	0.	0.
	1.079E+00	6.558E+01	0.	0.	0.
	0.				
delta-t	0.	0.	3.300E-02	3.160E-01	0.
	0.	0.	0.	0.	0.
	0.	0.	0.	0.	0.
	0.				
vt	0.	0.	0.	0.	0.
	0.	0.	0.	0.	0.
	0.	0.	1.000E+00	0.	0.
	0.				
wt	0.	0.	0.	0.	0.
	0.	0.	0.	0.	0.
	0.	0.	0.	1.000E+00	0.
	0.				
lambda	0.	0.	0.	0.	0.
	0.	0.	0.	0.	0.
	0.	0.	0.	0.	5.730E+01
	0.				
mu	0.	0.	0.	0.	0.
	0.	0.	0.	0.	0.
	0.	0.	0.	0.	0.
	5.730E+01				
lambda dot	0.	0.	-6.819E-02	0.	5.306E+00
	0.	-5.730E+01	0.	0.	0.
	0.	0.	6.819E-02	0.	0.
	-4.722E-02				
mu dot	0.	0.	0.	6.819E-02	-2.705E-01
	-5.730E+01	0.	0.	0.	0.
	0.	0.	0.	-6.819E-02	4.722E-02
	0.				
mu error	0.	-1.000E+00	0.	0.	0.
	0.	0.	0.	0.	0.

FIG. C.3 (Continued)

	0.	0.	0.	0.	0.
	5.730E+01				
mu err dot	-1.000E+00	5.000E-01	0.	6.819E-02	-2.705E-01
	-5.730E+01	0.	0.	0.	0.
	0.	0.	0.	-6.819E-02	4.722E-02
	0.				
pipper	0.	1.000E+00	0.	0.	0.
	0.	0.	0.	0.	0.
	0.	0.	0.	0.	0.
	0.				
pipper dot	1.000E+00	-5.000E-01	0.	0.	0.
	0.	0.	0.	0.	0.
	0.	0.	0.	0.	0.
	0.				

D MATRIX:

	delta-ep	delta-ap
u	0.	0.
v	0.	0.
w	0.	0.
p	0.	0.
q	0.	0.
r	0.	0.
theta	0.	0.
phi	0.	0.
az	-5.257E+00	0.
ay	0.	-9.017E-02
delta-e	-5.370E+00	0.
delta-a	0.	-1.580E+00
delta-r	0.	-9.017E-02
delta-t	0.	0.
vt	0.	0.
wt	0.	0.
lambda	0.	0.
mu	0.	0.
lambda dot	0.	0.
mu dot	0.	0.
mu error	0.	0.
mu err dot	0.	0.
pipper	0.	0.
pipper dot	0.	0.

EIGENVALUES

	REAL	IMAG	FREQ	DMPG
1	-2.500E-01	0.000E+00	2.500E-01	1.000E+00
2	-5.000E-01	0.000E+00	5.000E-01	1.000E+00
3	-5.563E+00	0.000E+00	5.563E+00	1.000E+00
4	-2.634E+00	1.771E+00	3.174E+00	8.299E-01
5	-2.634E+00	-1.771E+00	3.174E+00	8.299E-01
6	-3.216E+00	0.000E+00	3.216E+00	1.000E+00
7	-1.659E+00	0.000E+00	1.659E+00	1.000E+00
8	-4.643E-01	0.000E+00	4.643E-01	1.000E+00
9	-4.621E-03	1.328E-01	1.329E-01	3.476E-02
10	-4.621E-03	-1.328E-01	1.329E-01	3.476E-02
11	-1.480E-01	0.000E+00	1.480E-01	1.000E+00

FIG. C.3 (Continued)

12	-2.810E+00	0.000E+00	2.810E+00	1.000E+00
13	1.229E-06	8.249E-04	8.249E-04	-1.490E-03
14	1.229E-06	-8.249E-04	8.249E-04	-1.490E-03
15	-1.810E-04	0.000E+00	1.810E-04	1.000E+00
16	8.792E-06	0.000E+00	8.792E-06	-1.000E+00

FIG. C.3 (Concluded)

1. Report No.	2. Government Accession No.	3. Recipient's Catalog No.
NASA CR-172336		

4. Title and Subtitle	5. Report Date
F-14 Modeling Study	May 1984
	6. Performing Organization Code

7. Author(s)	8. Performing Organization Report No.
William H. Levison and Sheldon Baron	
	10. Work Unit No.

9. Performing Organization Name and Address	11. Contract or Grant No.
Bolt Beranek and Newman Inc. 10 Moulton Street Cambridge, MA 02238	NAS1-16738

12. Sponsoring Agency Name and Address	13. Type of Report and Period Covered
National Aeronautics and Space Administration Washington, DC 20546	Contractor report
	14. Sponsoring Agency Code 505-35-33-01

15. Supplementary Notes

Langley Technical Monitor: R. V. Parrish
Final Report

16. Abstract

In this report we describe preliminary results in the application of a closed-loop pilot/simulator model to the analysis of some simulator fidelity issues in the context of an air-to-air target tracking task. The closed-loop model is described briefly. Then, problem simplifications that are employed to reduce computational costs are discussed. Finally, model results showing sensitivity of performance to various assumptions concerning the simulator and/or the pilot are presented.

17. Key Words (Suggested by Author(s))	18. Distribution Statement
Simulation, modeling, pilot/ simulator model, simulator fidelity, motion, g-seat.	Unclassified-Unlimited Subject Category 05

19. Security Classif. (of this report)	20. Security Classif. (of this page)	21. No. of Pages	22. Price
Unclassified	Unclassified	95	A05

N-305 For sale by the National Technical Information Service, Springfield, Virginia 22161